SHARKEY, ANDREW, M.S., August 2026 APPLIED MATHEMATICS

MATHEMATICAL MODEL OF A REGENERATIVE FUEL CELL FOR SYSTEM OPTIMIZATION (52 pages)

Thesis Advisor: Dr. Xiaoyu Zheng

This thesis developed a system-level optimization model of a regenerative fuel cell (RFC) system for long-duration, off-world energy storage applications. Prior RFC design studies have typically been limited to reduced parameter sets and simplified constraints due to computational limitations relative to the number of relevant degrees of freedom. As a result, important nonlinear interactions between subsystems have not been fully captured. This work began to address that gap by developing a higher-fidelity, nonlinear optimization framework that incorporates a broader set of design variables and coupled constraints, enabling a multidimensional model that captures the coupled behavior of RFC subsystems and demonstrates the feasibility of applying optimization to such systems. An expanded system-level optimization approach was established that captures interactions between electrochemical performance, structural requirements, and storage design. This enabled a more comprehensive evaluation of trade-offs than conventional formulations.

The model integrates four coupled subsystems: a fuel cell, an electrolyzer, reactant gas, and high-pressure storage tanks, and was formulated to accommodate a wide range of mission parameters, including operational time and required output power. It incorporates constraints on available solar array power, reactant mass balance between production and consumption, and pressure-dependent storage requirements. To enable reliable convergence, the optimization problem was reformulated to reduce dimensionality and improve numerical stability, with subsystem models organized for efficient evaluation. Problem dimensionality was reduced by consolidating lower-level design variables into higher-level representative quantities, and subsystem behavior was evaluated within the optimization loop. A multi-start initialization strategy was employed to mitigate sensitivity to local minima and improve solution quality, while nonlinear relationships were solved using robust numerical methods. The results showed that convergence was achieved across a range of required output power values. Specific energy reached a maximum at a critical mission power level, where the electrolyzer power matched the available solar input and operated near its voltage and current density limits. Beyond this point, further increases in required power resulted

in less mass-efficient operation, increasing total system mass and reducing overall performance. The developed model represents an advancement in RFC system-level optimization by enabling analysis of a broader and more tightly coupled design space than previous considerations. While convergence behavior and computational cost remain challenges, the methods introduced improve solvability and allow inclusion of additional design variables with minimal loss of physical fidelity. However, the numerical results should not be interpreted as definitive design recommendations, as the model includes simplifying assumptions and omits several higher-order effects. Future work should extend this framework by incorporating additional subsystems and loss mechanisms, such as thermal management, parasitic power consumption, and reactant losses, to improve fidelity and ensure more representative design conclusions.

MATHEMATICAL MODEL OF A REGENERATIVE FUEL CELL FOR SYSTEM OPTIMIZATION

A thesis submitted

to Kent State University

in partial fulfillment of the requirements

for the degree of Master of Science

by

Andrew Sharkey

August 2026

Thesis written by

Andrew Sharkey

B.S., The University of Akron , 2023

M.S., Kent State University, 2026

Approved by

Dr. Xiaoyu Zheng _____, Chair, Master Thesis Committee

Dr. Jenya Soprunova _____, Chair, Department of Mathematical Sciences

Dr. Mandy Munro-Stasiuk _____, Dean, College of Arts and Sciences

TABLE OF CONTENTS

TABLE OF CONTENTS . . . . . **v**

LIST OF FIGURES . . . . . **vi**

LIST OF TABLES . . . . . **viii**

ACKNOWLEDGMENTS . . . . . **ix**

1 Introduction **1**

2 Mathematical Model **4**

2.1 Mass of the Fuel Cell 5

2.2 Mass of the Electrolyzer 7

2.3 Mass of Reactant Gases 11

2.3.1 Consumed Gases in the Fuel Cell 11

2.3.2 Produced Gases in the Electrolyzer 15

2.3.3 Reserved Gases 19

2.4 Mass of Storage Tanks 21

2.5 Model Summary 22

3 Results **27**

3.1 Algorithm 27

3.2 Numerical Results 30

4 Conclusion **35**

A Nomenclature **38**

BIBLIOGRAPHY **43**

LIST OF FIGURES

1 Example RFC System (adapted from [2]) 2

2 Fuel Cell Stack Diagram: (a) An individual FC stack, (b) Transverse section view of a single FC cell, and (c) Longitudinal section view of an FC cell. 5

3 Electrolyzer Stack Diagram: (a) An individual EZ stack, with clamping bolts shown on endplate, (b) Transverse section view of a single electrolyzer cell, and (c) Longitudinal section view of an EZ cell. 8

4 Electrolyzer Endplate Diagram 9

5 Fuel Cell Operation Graphs: (a) FC polarization curve, (b) FC power curve for different total active areas, (c) Contour plot of the mass of gas consumed. The pink and purple regions are where the fuel cell operates outside the ohmic region. The purple region corresponds to where the current density is too small, and the pink region corresponds to where the current density is too large. 13

6 Electrolyzer Operation Graphs: (a) Electrolyzer polarization curve, (b) Electrolyzer power density curve, (c) Contour plot of total system mass m_{sys} for electrolyzer pressure and total area. The purple region corresponds to where the electrolyzer high voltage constraint is violated, and the pink region corresponds to where the low current density constraint is violated. This graph corresponds to $P_{req} = 4000$ W, $A_{FC,tot} = 22500$ cm^2, and $p_{FC} = 1.2$ bar. 17

7 Compressibility Factor of H_2 and O_2 at 300 K 20

8 Spherical Tank Diagram 21

9 Fuel Cell and Electrolyzer Mapping Flowcharts. 28

10 Optimal fuel cell variables for range of total fuel cell area $A_{FC,tot}$. 28

11 Contours of optimal electrolyzer variables for range of total electrolyzer area $A_{EZ,tot}$ and electrolyzer pressure p_{EZ}. 29

12 (a) Flowchart of Algorithm for calculating system mass, (b) Flowchart of *fmincon*. . 29

13 System Properties VS Power: (a) Total System Mass, (b) System Specific Energy, (c) Total Active Areas of Stacks: $A_{FC,tot}$ and $A_{EZ,tot}$, (d) Stack Pressures: p_{FC} and p_{EZ}. 31
14 Total system mass contour plot. 31
15 Stack Design Variables VS Power: (a) Stack Power: P_{FC} and P_{EZ}, (b) Fuel Cell and Electrolyzer System Masses: m_{FC} and m_{EZ}, (c) Fuel Cell and Electrolyzer Current Densities: i_{FC} and i_{EZ}, (d) Fuel Cell and Electrolyzer Voltages: V_{FC} and V_{EZ}, (e) Individual Cell Area of Fuel Cell and Electrolyzer: A_{FC} and A_{EZ}, (f) Number of Cells per Stack of Fuel Cell and Electrolyzer: k_{FC} and k_{EZ}. 32
16 Tank and Reactant Gas Properties VS Power: (a) Total Reactant and Tank Mass (b) Consumed and Reserved Reactant Mass, (c) Tank Thickness, (d) Tank Radius, (e) Tank Volume, (f) Individual Tank Masses. 33

LIST OF TABLES

1 FC Constants 7

2 EZ Constants 10

3 Model Variables 23

4 Parameter Values at $P_{req} = 5400$ W, $P_{SA} = 10000$ W, $T_{EZ} = 351$ h, and $T_{FC} = 359$ h. 34

ACKNOWLEDGMENTS

The author would like to thank Dr. Xiaoyu Zheng for her patience and invaluable guidance in the development of this work, Ian Jakupca for providing the project and helping to define its scope, and Chris Heldman for his continued support. The author also thanks the Avionics and Photovoltaic and Electrochemical Conversion Branches at NASA for their continued support, and gratefully acknowledges the Ohio Space Grant Consortium and the Regenerative Fuel Cell Project at NASA Glenn Research Center for their financial support.

CHAPTER 1

Introduction

Existing off-world energy storage technologies face significant challenges in meeting the requirements for sustained operation through the lunar night. While several advanced energy storage options exist, the performance depends strongly on system-level integration and optimization across many coupled design parameters to maximize system-specific energy (Wh/kg). One such technology, the rechargeable regenerative fuel cell (RFC), uses electrochemistry and reactants to offer a path to a specific energy significantly higher than existing battery technologies used in space. An RFC requires coordinated design of the fuel cell, electrolyzer, reactant storage, and balance-of-plant components, rather than optimization of individual subsystems in isolation. As a result, RFC-based architectures are an active area of research for enabling long-duration surface operations in lunar environments [1].

An RFC is an electrochemical energy storage system that stores chemical energy in hydrogen and oxygen gases. It operates in two complementary modes: fuel cell mode, where electrical energy is discharged from the system, and electrolyzer mode, where the system is recharged with electrical energy supplied from an external power source.

In fuel cell mode, hydrogen and oxygen react electrochemically to generate electricity, heat, and water. The systems considered here employ proton exchange membrane (PEM) technology. Reactant storage tanks supply the gases to the fuel cell, supplying oxygen to the cathode and hydrogen to the anode. At the anode, a catalyst splits hydrogen into protons and electrons. The PEM allows the protons to pass through to the cathode, while not allowing the electrons through. By physically separating protons and electrons, the membrane sustains an electrical potential difference between the electrodes, which drives the electrons through the external circuit. This process enables the stored chemical energy of hydrogen and oxygen to be directly converted into electrical energy with water and heat as byproducts.

In electrolyzer mode, an external current source drives the dissociation of water within the electrolyzer stack. Water is supplied to the anode where it is oxidized when the cell voltage exceeds the reversible thermodynamic potential, plus the activation, ohmic, and mass-transport losses. This reaction produces oxygen gas, protons, and electrons. The protons migrate through the PEM to the cathode, while the electrons travel through the external circuit. At the cathode, the electrons combine with the protons to form hydrogen gas. This process converts electrical energy into chemical energy stored in the form of hydrogen and oxygen reactants, which can later be used by the fuel cell to generate electricity and water.

By cycling between these two modes, the RFC produces and stores reactant gases during periods of high energy generation and later uses the reactant gases to produce electrical power during periods of high demand.

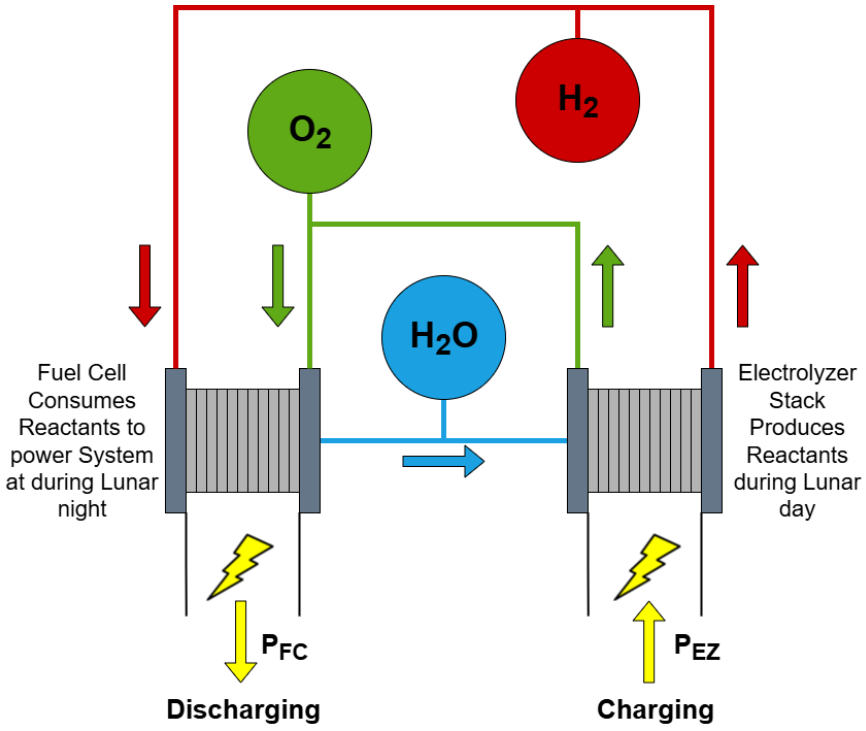

Figure 1: Example RFC System (adapted from [2])

Unlike a battery, which stores a fixed amount of energy in internal electrode materials, an RFC stores energy separately from the energy conversion mechanism. Because its energy capacity is determined by the size of the reactant tanks rather than the cell stack, the RFC can achieve much higher specific energy than batteries, making it especially suited for applications where high specific

energy (energy per mass) is critical.

The goal of this project is to develop a robust and integrated model of the regenerative fuel cell system, considering operational characteristics of the fuel cell, electrolysis, and fluidic systems within a lunar environment to accurately estimate the system's specific energy for optimization purposes. In addition, we seek to apply optimization algorithms to identify critical design parameters that maximize specific energy of the RFC system by conducting a sensitivity analysis.

Several effects were not included in this study. During fuel cell and electrolyzer operation, back-diffusion and reactant crossover losses were neglected in the calculation of gas consumption and production. In addition, losses during storage, such as leakage or venting, were not accounted for in the reactant mass or tank sizing. The model also excludes electrical power management and thermal control subsystems, as well as detailed fluidic components such as pumps and valves, all of which would contribute non-negligible mass. Finally, parasitic power consumption during operation was not considered, so the net usable power would be lower than predicted.

The remainder of this thesis is organized as follows. Chapter 2 presents the system-level model of the regenerative fuel cell, including the mass calculations of the fuel cell, electrolyzer, reactant mass, and storage tanks, together with power, mass-balance, and structure constraints. Chapter 3 describes the optimization methodology and presents the numerical results. Chapter 4 summarizes the main conclusions of the work.

CHAPTER 2

Mathematical Model

The model seeks to maximize the system's specific energy (SE) per cycle, defined as

$$SE = \frac{1}{m_{sys}} \int_0^{T_{FC}} (P_{Req} - P_{cons}) dt. \tag{2.1}$$

Here, T_{FC} denotes the operation time per cycle for the fuel cell (FC). The term P_{Req} is the required gross power supplied by the FC during its operation, while P_{cons} accounts for any internal power consumed during the FC operation. In this study, we assume $P_{cons} = 0$ and treat T_{FC} and P_{Req} as fixed parameters. Furthermore, P_{Req} is considered a constant during the FC operation, which simplifies the integral in Eq. (2.1), and the specific energy per cycle reduces to:

$$SE = \frac{1}{m_{sys}} P_{Req} T_{FC}. \tag{2.2}$$

In the above expression, the total system mass m_{sys} plays a key role and is composed of four main parts:

$$m_{sys} = m_{FC} + m_{EZ} + m_{Gas} + m_{BoP}, \tag{2.3}$$

where m_{FC} is the mass of the fuel cell, m_{EZ} is the mass of the electrolyzer, m_{Gas} is the mass of the stored reactant gases (hydrogen and oxygen), and m_{BoP} is the mass of the balance-of-plant (BoP), consisting of tanks for the storage of hydrogen, oxygen, and water.

To limit the scope of our study, we only vary certain fuel cell stack and electrolyzer stack parameters for optimization, specifically, the number of stacks (N_{FC} and N_{EZ}), the number of cells per stack (k_{FC} and k_{EZ}), the areas of each cell (A_{FC} and A_{EZ}), and the operating pressure of the stacks (p_{FC} and p_{EZ}). Thus we have a model which takes these eight variables, as well as any necessary parameters (operation time T_{FC}, required power P_{Req}, fuel cell and electrolyzer parameters) and predicts the masses of the system.

Throughout this thesis, we use centimeters (cm) for length, kilograms (kg) for mass, watts (W) for power, and bars for pressure.

We now turn to modeling the mass contributions of each primary component: the fuel cell, the electrolyzer, the reactant gases, and the water/gas storage containers.

2.1 Mass of the Fuel Cell

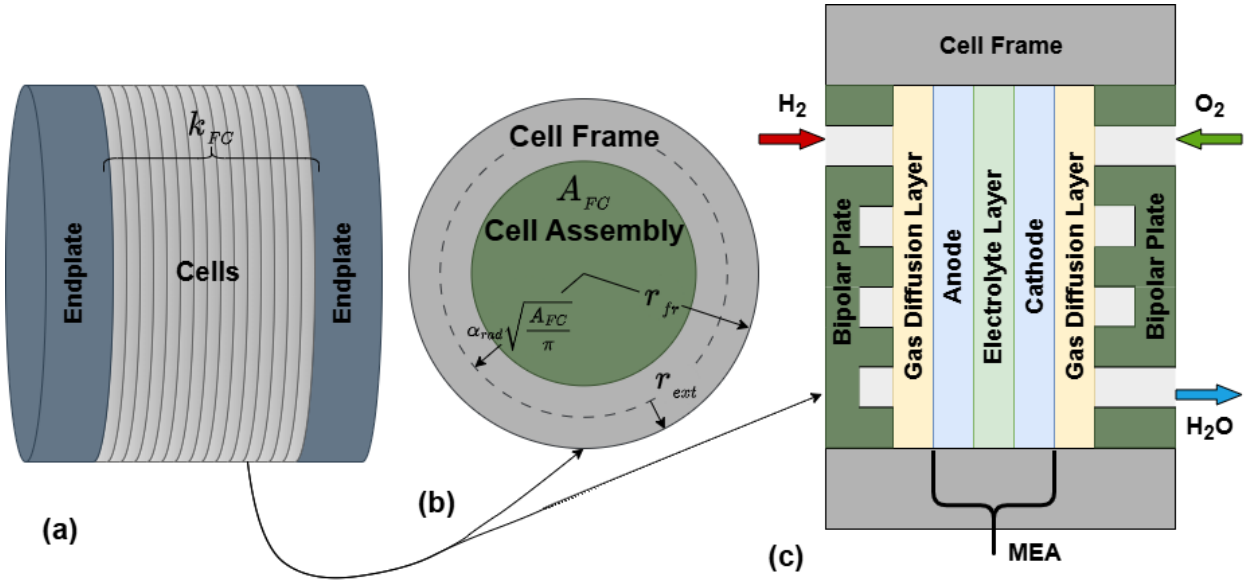

Figure 2: Fuel Cell Stack Diagram: (a) An individual FC stack, (b) Transverse section view of a single FC cell, and (c) Longitudinal section view of an FC cell.

The mass of the fuel cell system is determined by summing the contributions of key components at both the cell and stack levels, accounting for both the fuel cell's structural layout and the combined system layout:

$$m_{FC} = 1.2 \cdot N_{FC} \left(k_{FC} \left(m_{MEA}^{FC} + m_{bp}^{FC} + m_{fr}^{FC} \right) + 2m_{ep}^{FC} + m_{aux}^{FC} \right), \tag{2.4}$$

where N_{FC} is the total number of fuel cell stacks. The parameter k_{FC} represents the number of cells per stack, as shown in Fig. 2(a).

The mass of each individual fuel cell is comprised of three main components: m_{MEA}^{FC}, m_{bp}^{FC}, and m_{fr}^{FC}. Specifically, m_{MEA}^{FC} is the mass of the cell membrane electrode assembly (MEA), where the electrochemical reactions take place; m_{bp}^{FC} is the mass of the bipolar plate, which separates adjacent cells and directs the gases along the MEA; and m_{fr}^{FC} is the mass of the cell frame. Assuming a

circular geometry, the primary per-cell masses are calculated as follows:

$$m_{MEA}^{FC} = \sigma_{MEA}^{FC} A_{FC}, \tag{2.5}$$

$$m_{bp}^{FC} = \rho_{bp}^{FC} A_{FC} t_{bp}^{FC}, \tag{2.6}$$

$$m_{fr}^{FC} = \rho_{fr}^{FC} \left(\pi \left(r_{fr}^{FC} \right)^2 - A_{FC} \right) t_{fr}^{FC}, \tag{2.7}$$

where A_{FC} is the area of each cell, and σ_{MEA}^{FC} is the area density of the MEA. The bipolar plate has thickness t_{bp}^{FC} and density ρ_{bp}^{FC}, while the cell frame has the thickness t_{fr}^{FC} and density ρ_{fr}^{FC}. The outer radius of the frame, r_{fr}^{FC}, is derived from the fuel cell area and is given by

$$r_{fr}^{FC} = \alpha_{FC} \cdot \sqrt{\frac{A_{FC}}{\pi}} + r_{ext}^{FC}, \tag{2.8}$$

where α_{FC} is the geometric scaling factor and r_{ext}^{FC} is the additional fixed radial extension of the cell frame.

The next term in Eq. (2.4) is m_{ep}^{FC}, which represents the mass of the fuel cell endplates, which clamp the cells together. The mass of each endplate is computed as

$$m_{ep}^{FC} = \rho_{ep}^{FC} \pi \left(r_{fr}^{FC} \right)^2 t_{ep}^{FC}, \tag{2.9}$$

where ρ_{ep}^{FC} and t_{ep}^{FC} are the density and thickness of the endplate, respectively, and the radii of the endplates are the same as the cell frame r_{fr}^{FC}.

The term m_{aux}^{FC} accounts for auxiliary masses such as wires and piping that are needed for each fuel cell stack, while the factor 1.2 is included to approximate the mass of auxiliary cells such as humidifiers or degasser cells, which are used to control the performance of the fuel cell.

By combining the expressions above, the fuel cell system mass can be re-expressed in the form:

$$m_{FC}(N_{FC}, k_{FC}, A_{FC}) = N_{FC} \left(a_1 A_{FC} k_{FC} + a_2 \sqrt{A_{FC}} k_{FC} + a_3 A_{FC} + a_4 \sqrt{A_{FC}} + a_5 k_{FC} + a_6 \right), \tag{2.10}$$

where a_1 through a_6 are constants derived from the fuel cell's physical parameters. The terms involving $\sqrt{A_{FC}}$ arise due to the dependence on the cell radius. Using the parameter values listed in Appendix A, the specific values of these constants are given in Table 1.

In this model, we assume the effect of the fuel cell pressure on the fuel cell mass is negligible by limiting the pressure to be low. Although the fuel cell pressure has a negligible effect on the

Table 1: FC Constants

	a_1	a_2	a_3	a_4	a_5	a_6
Units	$\frac{kg}{cm^2}$	$\frac{kg}{cm}$	$\frac{kg}{cm^2}$	$\frac{kg}{cm}$	kg	kg
Value	0.0021	0.0050	0.0111	0.0536	0.0088	10.0176

fuel cell mass, it does have an effect on other masses in the system. Thus we have some constraints that dictate the design of the fuel cell:

$$1 \leq \quad N_{FC} \quad \leq 10, \tag{2.11}$$

$$1 \leq \quad k_{FC} \quad \leq 200, \tag{2.12}$$

$$1 \text{ cm}^2 \leq \quad A_{FC} \quad \leq 2000 \text{ cm}^2, \tag{2.13}$$

$$1.2 \text{ bar} \leq \quad p_{FC} \quad \leq 7 \text{ bar}. \tag{2.14}$$

As shown later in Section 2.3.1, the total gas consumed in the FC is proportional to the total active area,

$$A_{FC,tot} = N_{FC} k_{FC} A_{FC}. \tag{2.15}$$

For a fixed total active area, the FC mass is minimized when $N_{FC} = 1$, provided that k_{FC} and A_{FC} remain within their allowable ranges. This can be easily seen because if $N_{FC} > 1$, the total auxiliary mass is multiplied. In addition, the terms with coefficients a_2 and a_4 in Eq. (2.10) scale as $A_{FC}^{1/2}$, favoring a larger A_{FC} and a smaller k_{FC} for minimum FC mass.

2.2 Mass of the Electrolyzer

The electrolyzer mass equation has similar structure as that of the fuel cell with a few differences:

$$m_{EZ} = N_{EZ} \left(k_{EZ} \left(m_{MEA}^{EZ} + m_{sc,an}^{EZ} + m_{sc,ca}^{EZ} + m_{fr}^{EZ} \right) + 2m_{ep}^{EZ} + k_{bolt}^{EZ} m_{bolt}^{EZ} + m_{aux}^{EZ} \right), \tag{2.16}$$

where N_{EZ} is the total number of electrolyzer stacks and k_{EZ} is the number of cells per stack.

Each electrolyzer cell consists of a MEA with mass m_{MEA}^{EZ} and a frame with mass m_{fr}^{EZ}. In place of a bipolar plate, an anode screen $m_{sc,an}^{EZ}$ and a cathode screen $m_{sc,ca}^{EZ}$ are used to distribute fluids across the cell. A thin separator between adjacent screens prevents reactant crossover; its mass is

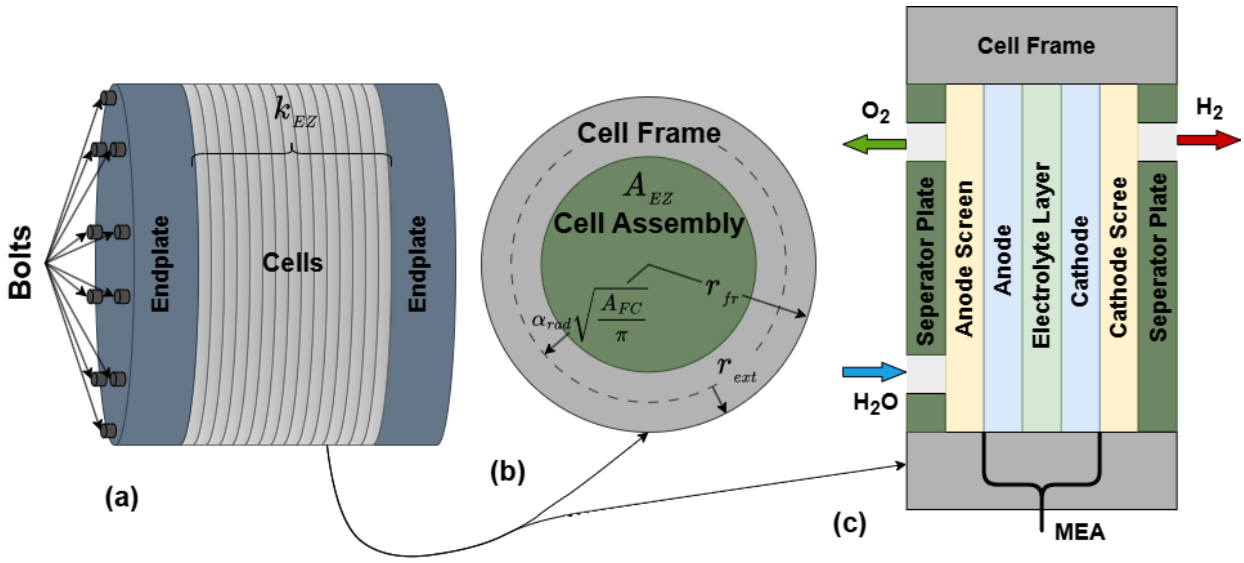

Figure 3: Electrolyzer Stack Diagram: (a) An individual EZ stack, with clamping bolts shown on endplate, (b) Transverse section view of a single electrolyzer cell, and (c) Longitudinal section view of an EZ cell.

considered negligible. As with the fuel cell, electrolyzer cells are modeled with circular geometry, and the component masses are calculated as follows:

$$m_{MEA}^{EZ} = \sigma_{MEA}^{EZ} A_{EZ}, \tag{2.17}$$

$$m_{sc,an}^{EZ} = \left(1 - \phi_{sc,an}^{EZ}\right) \rho_{sc,an}^{EZ} A_{EZ} t_{sc,an}^{EZ}, \tag{2.18}$$

$$m_{sc,ca}^{EZ} = \left(1 - \phi_{sc,ca}^{EZ}\right) \rho_{sc,ca}^{EZ} A_{EZ} t_{sc,ca}^{EZ}, \tag{2.19}$$

$$m_{fr}^{EZ} = \rho_{fr}^{EZ} (\pi \left(r_{fr}^{EZ}\right)^2 - A_{EZ}) t_{fr}^{EZ}. \tag{2.20}$$

Here, A_{EZ} denotes the area of each cell. The densities of the frame, anode screen, cathode screen and MEA are ρ_{fr}^{EZ}, $\rho_{sc,an}^{EZ}$, $\rho_{sc,ca}^{EZ}$, and ρ_{MEA}^{EZ}, respectively; their corresponding thicknesses are t_{fr}^{EZ}, $t_{sc,an}^{EZ}$, $t_{sc,ca}^{EZ}$, and t_{MEA}^{EZ}. The porosities of the anode and cathode screens are $\phi_{sc,an}^{EZ}$ and $\phi_{sc,ca}^{EZ}$, respectively. The outer frame radius r_{fr}^{EZ} is computed from the cell area as

$$r_{fr}^{EZ} = \alpha_{EZ} \sqrt{\frac{A_{EZ}}{\pi}} + r_{ext}^{EZ}, \tag{2.21}$$

where α_{EZ} is a geometric scaling factor and r_{ext}^{EZ} is the fixed radial extension of the frame.

The mass of the endplate is

$$m_{ep}^{EZ} = \rho_{ep}^{EZ} \pi \left(r_{fr}^{EZ}\right)^2 t_{ep}^{EZ}, \tag{2.22}$$

where ρ_{ep}^{EZ} is the endplate density, t_{ep}^{EZ} is the endplate thickness, and r_{fr}^{EZ} is the endplate radius, which is equivalent to the previously discussed frame radius. Unlike the fuel cell, the electrolyzer operates at considerably higher pressure; therefore the endplate thickness t_{ep}^{EZ} must be sufficient to ensure the maximum deflection of the endplate does not exceed the limit δ_{max}, preventing leakage of reactant gas. Using the deflection formula for a simply supported circular plate under uniform pressure (see Fig. 4), the required thickness is [3]

$$t_{ep}^{EZ} = \left(\frac{12 p_{EZ} \left(r_{fr}^{EZ} \right)^4 \left(1 - \nu^2 \right)}{64 \delta_{max} E} \right)^{1/3}. \tag{2.23}$$

Here, ν is Poisson's ratio and E is the elastic modulus of the endplate material.

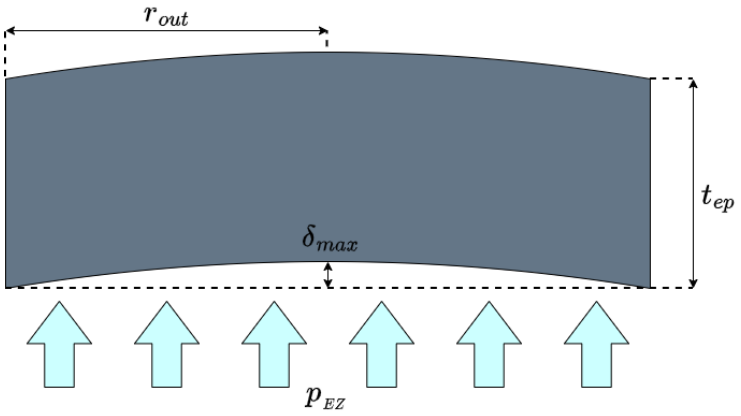

Figure 4: Electrolyzer Endplate Diagram

The next term in Eq. (2.16) is the mass of the clamping bolts. The bolts are distributed evenly around the perimeter of each stack. Each bolt is modeled as a cylinder, so its mass is

$$m_{bolt}^{EZ} = \rho_{bolt}^{EZ} \pi \left(r_{bolt}^{EZ} \right)^2 t_{total}^{EZ}, \tag{2.24}$$

where r_{bolt}^{EZ} and ρ_{bolt}^{EZ} are the bolt radius and density, respectively. The bolt radius is assumed to be $r_{bolt}^{EZ} = 1.27$ cm.

The total bolt length is the stack length plus an allowance for clamping:

$$t_{total}^{EZ} = 2t_{ep}^{EZ} + k_{EZ} \left(t_{fr}^{EZ} + t_{sc,an}^{EZ} + t_{sc,ca}^{EZ} + t_{MEA}^{EZ} \right) + 5. \tag{2.25}$$

The number of bolts is chosen so that the total clamping force exceeds the pressurization force on

the stack [4]:

$$k_{bolt}^{EZ} = \left\lceil \frac{6 p_{EZ} A_{EZ}}{s} \right\rceil, \tag{2.26}$$

where s is the maximum clamp force provided by a single bolt and the factor 6 is a safety factor. Here $\lceil \cdot \rceil$ denotes the ceiling function (rounding up to the nearest integer).

The term m_{aux}^{EZ} accounts for auxiliary masses such as wires and piping that are needed for each electrolyzer stack.

Combining all governing relations, the electrolyzer system mass can be expressed as a function of the design variables N_{EZ}, k_{EZ}, A_{EZ}, and p_{EZ} as

$$\begin{aligned} m_{EZ}(N_{EZ}, k_{EZ}, A_{EZ}, p_{EZ}) = N_{EZ} \Big(& b_1 k_{EZ} A_{EZ} + b_2 k_{EZ} \left(r_{fr}^{EZ}\right)^2 + b_3 A_{EZ} p_{EZ} k_{EZ} + b_4 A_{EZ} p_{EZ} \\ & + b_5 A_{EZ} p_{EZ}^{4/3} \left(r_{fr}^{EZ}\right)^{4/3} + b_6 p_{EZ}^{1/3} \left(r_{fr}^{EZ}\right)^{10/3} + b_7 \Big). \end{aligned} \tag{2.27}$$

with

$$r_{fr}^{EZ}(A_{EZ}) = \alpha_{EZ} \sqrt{\frac{A_{EZ}}{\pi}} + r_{ext}^{EZ}. \tag{2.28}$$

Here b_1 through b_7 are constants derived from the electrolyzer physical characteristics. Using the parameter values listed in Appendix A, the specific values of these constants are given in Table 2.

Table 2: EZ Constants

	b_1	b_2	b_3	b_4	b_5	b_6	b_7
Units	$\frac{kg}{cm^2}$	kg	$\frac{kg}{N}$	$\frac{kg}{N}$	$\frac{kg}{N^{4/3}cm^2}$	$\frac{kg}{N^{1/3}cm^{8/3}}$	kg
Value	0.00070	0.00101	$1.3040 \cdot 10^{-6}$	$1.1954 \cdot 10^{-5}$	$1.1841 \cdot 10^{-11}$	0.00029	10

In addition to these equations, we also have some constraints on the sizing of the electrolyzer. First, we require N_{EZ}, k_{EZ}, A_{EZ} and p_{EZ} to lie within a feasible range:

$$1 \leq \quad N_{EZ} \quad \leq 10, \tag{2.29}$$

$$1 \leq \quad k_{EZ} \quad \leq 200, \tag{2.30}$$

$$1 \text{ cm}^2 \leq \quad A_{EZ} \quad \leq 2000 \text{ cm}^2, \tag{2.31}$$

$$30 \text{ bar} \leq \quad p_{EZ} \quad \leq 350 \text{ bar}, \tag{2.32}$$

The gas produced by EZ is proportional to the total active area of the electrolyzer $A_{EZ,tot}$, which is given by

$$A_{EZ,tot} = N_{EZ} k_{EZ} A_{EZ}. \tag{2.33}$$

Given a value of $A_{EZ,tot}$, we can draw some rough insights into the three independent variables, k_{EZ}, A_{EZ}, and N_{EZ}. When the electrolyzer pressure is moderate to low, we can expect the EZ mass to be minimized when $N_{EZ} = 1$, since if $N_{EZ} > 1$ the total mass is multiplied. When the electrolyzer pressure is high, the terms involving p_{EZ} become significant, and terms with coefficients b_5 and b_6 scale with $A^{5/3}$, favoring a smaller area and consequently a larger N_{EZ}. Thus we will see $N_{EZ} > 1$ for high pressure.

2.3 Mass of Reactant Gases

The total mass of gases is expressed as

$$m_{Gas}(N_{FC}, k_{FC}, A_{FC}, p_{FC}, p_{EZ}) = m_{H_2,cons} + m_{O_2,cons} + m_{H_2,res} + m_{O_2,res}. \tag{2.34}$$

where $m_{H_2,cons}$ and $m_{O_2,cons}$ are the masses of hydrogen and oxygen consumed by the fuel cell during operation. The reserve terms, $m_{H_2,res}$ and $m_{O_2,res}$, represent the residual gas that must remain in the tanks to prevent reverse flow from the fuel cell back into the storage system.

This section is divided into three parts. First, we discuss the operation of the fuel cell and the reactant gases it consumes. Next, we examine the operation of the electrolyzer and the mass of gases produced during electrolyzer operation. Finally, we consider the reserve gases required to provide back pressure to the fuel cell.

2.3.1 Consumed Gases in the Fuel Cell

To meet a given power demand, a PEM (proton exchange membrane) fuel cell converts the chemical energy of hydrogen and oxygen into electrical energy through their electrochemical reaction. At the anode, hydrogen reacts with a catalyst, splitting the H_2 molecule into electrons and protons. The electrolyte membrane conducts protons from the anode to the cathode while preventing the passage of electrons, which instead pass around the membrane by passing through the external circuit. At the cathode, oxygen molecules combine with the protons and the returning electrons to form water. The physical separation of charge created by the membrane, electrons at the anode, positive ions at the cathode, creates an electrical potential difference between the two electrodes. This potential

difference, or voltage (V_{FC}), provides the electromotive force to drive electrons through an external circuit, creating a spontaneous current that performs electrical work.

The electrical power, P_{FC}, produced by this process is the product of the total current and the operating voltage. Because of the constant power assumption, the fundamental operating constraint that must be satisfied is [5]:

$$P_{FC} = i_{FC} V_{FC} A_{FC,tot} = P_{req}, \tag{2.35}$$

where $A_{FC,tot}$ is the total active area of the fuel cell, i_{FC} is the fuel cell current density, and V_{FC} is the voltage of each cell.

We can calculate the rate of electron flow from the total current flow of the fuel cell [5]:

$$\dot{n}_e = \frac{A_{FC,tot} i_{FC}}{F}, \tag{2.36}$$

where $\dot{n}_e$ is the total rate of electron transfer in the fuel cell, and Faraday's constant, $F = 96485.3321\ \mathrm{A \cdot s/mol}$, gives the charge carried by one mole of electrons.

The rate of consumption of the hydrogen and oxygen mass is directly proportional to the electron flow, thus the total consumed masses can be found using the total operation time of the fuel cell T_{FC} [5]:

$$m_{H_2,cons} = \frac{M_{H_2}}{n_{H_2}} \dot{n}_e T_{FC} = \frac{M_{H_2}}{n_{H_2} F} A_{FC,tot} i_{FC} T_{FC}, \tag{2.37}$$

$$m_{O_2,cons} = \frac{M_{O_2}}{n_{O_2}} \dot{n}_e T_{FC} = \frac{M_{O_2}}{n_{O_2} F} A_{FC,tot} i_{FC} T_{FC}, \tag{2.38}$$

Here, $M_{H_2} = 2.0159\ \mathrm{g/mol}$ and $M_{O_2} = 31.9988\ \mathrm{g/mol}$ are the molar masses of hydrogen and oxygen, respectively. The coefficients $n_{H_2} = 2$ and $n_{O_2} = 4$ represent the moles of electrons transferred per mole of hydrogen and oxygen consumed.

We can rewrite Eq. (2.37) and (2.38) using Eq. (2.35) to get the reactant mass in terms of the fuel cell voltage and power:

$$m_{H_2,cons} = \frac{M_{H_2}}{n_{H_2} F} \frac{P_{req}}{V_{FC}} T_{FC}, \tag{2.39}$$

$$m_{O_2,cons} = \frac{M_{O_2}}{n_{O_2} F} \frac{P_{req}}{V_{FC}} T_{FC}. \tag{2.40}$$

A critical insight from Eqs. (2.39) and (2.40) is that for a fixed power requirement P_{req}, and fixed time T_{FC}, the mass of gas consumed is minimized by operating the fuel cell at the highest

allowable voltage. Therefore, the problem of minimizing the total reactant mass consumed for a given mission is fundamentally a problem of maximizing the operational cell voltage, subject to the equality constraint imposed by the power requirement in Eq. (2.35).

The fuel cell voltage V_{FC}, in Eqs. (2.39) and (2.40), is a function of the current density i_{FC} and the fuel cell pressure p_{FC}, and is described by the polarization curve [5]:

$$V_{FC}(i_{FC}, p_{FC}) = V_{rev}(p_{FC}) - \beta_{FC} \ln\left(\frac{i_{FC} + i_{FC,offset}}{i_{FC,0}}\right) - i_{FC} R_{FC} - c_{FC} \ln\left(\frac{i_{FC,lim}}{i_{FC,lim} - i_{FC}}\right), \quad (2.41)$$

where the first term, V_{rev}, is the maximum achievable voltage, and the second through fourth terms are the inefficiencies of the fuel cell stack. An example fuel cell polarization curve, V_{FC} versus i_{FC}, is shown in Fig. 5(a) for representative fuel cell pressures p_{FC}.

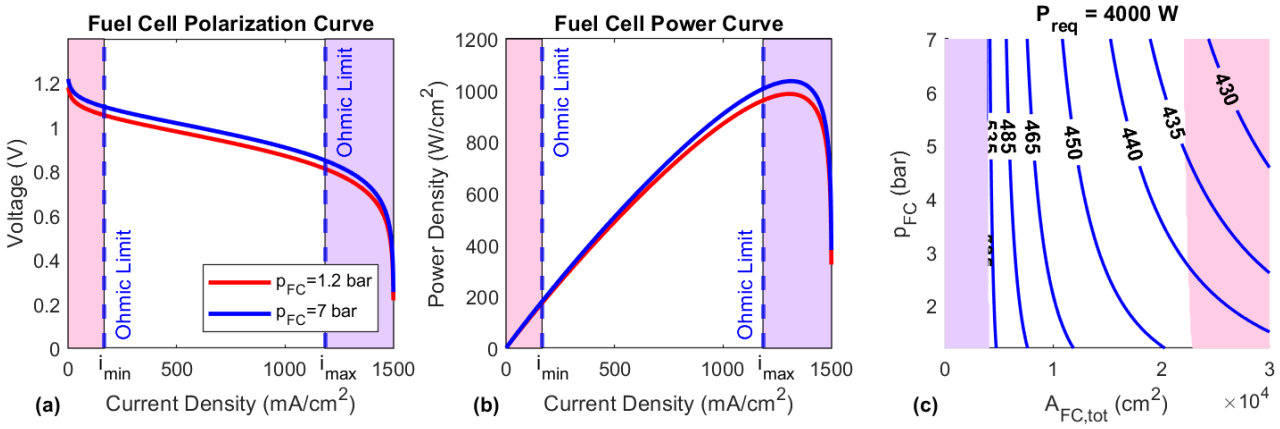

Figure 5: Fuel Cell Operation Graphs: (a) FC polarization curve, (b) FC power curve for different total active areas, (c) Contour plot of the mass of gas consumed. The pink and purple regions are where the fuel cell operates outside the ohmic region. The purple region corresponds to where the current density is too small, and the pink region corresponds to where the current density is too large.

The reversible voltage V_{rev} accounts for the pressure and temperature of the fuel cell, and the energy release during the chemical reaction:

$$V_{rev}(p_{FC}) = -\frac{\Delta G_F}{2F} + \frac{R T_{temp}}{2F} \ln\left(\frac{\frac{p_{H_2}}{p_0}\left(\frac{p_{O_2}}{p_0}\right)^{\frac{1}{2}}}{\frac{p_{H_2O}}{p_0}}\right). \quad (2.42)$$

The first term accounts for the change in Gibbs free energy of formation of water, ΔG_F, which quantifies the energy released when hydrogen and oxygen combine to form water under standard-

state conditions. The standard state corresponds to $T = 25°\text{C}$ and $P = 1$ bar, for which $\Delta G_{_F} = -237.14$ kJ/mol. The negative value indicates that the reaction is spontaneous and releases energy. The second term is the Nernst correction, which adjusts the voltage based on deviations from standard-state conditions by accounting for the effect of temperature and reactant/product partial pressures. Here R is the universal gas constant, and $T_{_{temp}}$ is the operating temperature. The partial pressures $p_{_{H_2}}$, $p_{_{O_2}}$, and $p_{_{H_2O}}$ represent the pressures exerted by each species and p_0 is the reference pressure, which is 1 atm. For pure reactant gases, the partial pressures are equal to the operating fuel cell pressure $p_{_{H_2}} = p_{_{O_2}} = p_{_{FC}}$. Since the model assumes liquid water as the product, the partial pressure of water vapor is fixed at one atmosphere, $p_{_{H_2O}} = 1$ atm $= 1.01325$ bar.

Together, the second through fourth terms in Eq. (2.41) quantify the different sources of energy loss, or inefficiencies, in the fuel cell. The second term corresponds to the activation loss of the system, which is the voltage drop in a fuel cell caused by the energy required to initiate the electrochemical reactions at the electrodes. In this term, $\beta_{_{FC}}$ is the Tafel slope parameter, $i_{_{FC,0}}$ is the reference current, and $i_{_{FC,offset}}$ is the current density correction. These parameters depend on the specific design and manufacturing of the fuel cell. The third term represents the ohmic loss of the fuel cell, which includes the electrical resistance to electron flow and the ionic resistance to proton flow across the fuel cell membrane. Here $R_{_{FC}}$ represents the combined resistance of the fuel cell. The final term is the concentration loss of the fuel cell system, which corresponds to the voltage drop caused by limitations in mass transport when reactants cannot reach the electrodes fast enough at high current densities. Here $i_{_{FC,lim}}$ is the limiting current density of the fuel cell, and $c_{_{FC}}$ is the reactant concentration factor.

The efficiency of the fuel cell can be described using the actual power out divided by the ideal power out:

$$\eta_{_{FC}} = \frac{P_{_{FC}}}{P_{_{ideal}}} = \frac{V_{_{FC}}\, i_{_{FC}}\, A_{_{FC,tot}}}{V_{_{rev}}\, i_{_{FC}}\, A_{_{FC,tot}}} = \frac{V_{_{FC}}}{V_{_{rev}}}. \tag{2.43}$$

Therefore, high efficiency is achieved at high voltage and low current density. Since the mass consumed by the fuel cell is inversely proportional to the cell voltage $V_{_{FC}}$, as shown in Eq. (2.39), the fuel cell will consume the least gas when operating at highest efficiency.

For proper operation, the fuel cell current density must be maintained within a range that keeps the cell predominantly in the ohmic region of the polarization curve, avoiding excessive activation

or concentration losses. This admissible range can be approximated by ensuring that the second derivative of the polarization curve with respect to i_{FC} remains below a specified tolerance, ϵ, giving:

$$i_{FC} \in \left[\sqrt{\frac{\beta_{FC}}{\epsilon}} - i_{FC,offset},\ i_{FC,lim} - \sqrt{\frac{c_{FC}}{\epsilon}} \right]. \tag{2.44}$$

With the feasible region defined, Fig. 5(b) shows how fuel cell power varies with current density. Because voltage decreases as current density increases, lower current densities correspond to higher efficiency. For a given power output, increasing $A_{FC,tot}$ reduces the power density, which improves efficiency and lowers reactant gas consumption. This behavior is illustrated in Fig. 5(c), where the consumed gas mass is plotted as a function of $A_{FC,tot}$ and pressure p_{FC}. The minimum gas consumption occurs when both pressure and active area are maximized, within the bounds of operating constraints.

Minimizing gas consumption alone does not necessarily yield the lowest total system mass. Increasing the total fuel cell area $A_{FC,tot}$ reduces gas usage by lowering the operating current density, but it also increases the fuel cell stack mass. In most operating regimes, the impact of consumed gas mass dominates over the stack mass, except at low power levels. This drives the design toward a maximum fuel cell area that keeps the current density i_{FC} within the feasible region. Similarly, increasing the fuel cell operating pressure p_{FC} reduces reactant consumption by improving cell performance, but it also increases the required reserve gas mass and storage tank mass, as discussed in Sections 2.3.3 and 2.4. Therefore, the optimal fuel cell pressure arises from balancing these competing effects (stack mass, consumed gas, and reserve storage) rather than simply maximizing or minimizing any single parameter. The resulting tradeoffs in operating pressure are examined further in Section 2.3.3.

2.3.2 Produced Gases in the Electrolyzer

Whereas a fuel cell converts chemical energy into electricity, a PEM electrolyzer performs the reverse process, using electrical energy to produce chemical energy in the form of hydrogen and oxygen. When a current source is applied across the electrodes, water at the anode is dissociated on a catalytic surface, releasing oxygen, protons, and electrons. Just like the fuel cell, the membrane selectively conducts the protons to the cathode while the electrons pass around the membrane through the external circuit. At the cathode, these protons recombine with electrons to form

hydrogen gas, while the oxygen is left at the anode, where it is separated from the input water and directed to the gas storage tank.

The hydrogen produced by the electrolyzer should be equal to the hydrogen consumed by the fuel cell,

$$m_{H_2,prod} = m_{H_2,cons}. \tag{2.45}$$

Because the oxygen consumption is stoichiometrically proportional to the hydrogen consumption, a separate constraint on oxygen production is unnecessary. Similar to the fuel cell, the reactant mass production is determined by the rate of the electron transfer, which is dependent on the electrolyzer current density i_{EZ} and the total active area $A_{EZ,tot}$:

$$\dot{n}_e = \frac{A_{EZ,tot} i_{EZ}}{F}, \tag{2.46}$$

where $\dot{n}_e$ is the total rate of electron transfer in the electrolyzer, and F is Faraday's constant. The mass of hydrogen produced by the electrolyzer is given by

$$m_{H_2,prod} = \frac{M_{H_2}}{n_{H_2}} \dot{n}_e T_{EZ} = \frac{M_{H_2}}{n_{H_2} F} A_{EZ,tot} i_{EZ} T_{EZ}, \tag{2.47}$$

where T_{EZ} is the electrolyzer operating time, treated here as a given parameter. The molar mass of hydrogen is $M_{H_2} = 2.0159$ g/mol and $n_{H_2} = 2$ is the number of moles of electrons transferred per mole of hydrogen produced. Combining Eq. (2.47) and the equality constraint Eq. (2.45) yields a relationship between the electrolyzer operating variables and parameters and those of the fuel cell,

$$i_{EZ} A_{EZ,tot} T_{EZ} = i_{FC} A_{FC,tot} T_{FC}. \tag{2.48}$$

For a given electrolyzer total area $A_{EZ,tot}$, Eq. (2.48) can be rearranged to determine the electrolyzer current density i_{EZ}:

$$i_{EZ} = i_{FC} \frac{A_{FC,tot} T_{FC}}{T_{EZ} A_{EZ,tot}}. \tag{2.49}$$

The electrical power consumed by the electrolyzer stack is

$$P_{EZ} = i_{EZ} V_{EZ} A_{EZ,tot}, \tag{2.50}$$

where V_{EZ} is the voltage of each electrolyzer cell. The electrolyzer power consumption P_{EZ} is limited by the maximum power supplied by the solar array,

$$P_{EZ} \leq P_{SA}, \tag{2.51}$$

where P_{SA} denotes the maximum available solar array power.

Similar to the fuel cell, the electrolyzer voltage depends on the current density, reflecting the energy required to split water into hydrogen and oxygen. The minimum required voltage is given by the Gibbs free energy of formation, represented by the reversible voltage V_{rev}, while additional voltage is required to overcome electrochemical losses. The polarization curve for the electrolyzer is expressed as [6, 5]

$$V_{EZ}(i_{EZ}, p_{EZ}) = V_{rev}(p_{EZ}) + \beta_{EZ} \ln\left(\frac{i_{EZ} + i_{EZ,offset}}{i_{EZ,0}}\right) + i_{EZ} R_{EZ} + c_{EZ} \ln\left(\frac{i_{EZ,lim}}{i_{EZ,lim} - i_{EZ}}\right), \quad (2.52)$$

where the reversible voltage V_{rev} is calculated in the same manner as the fuel cell in Eq. (2.42), replacing the pressure p_{FC} with the electrolyzer operating pressure p_{EZ}.

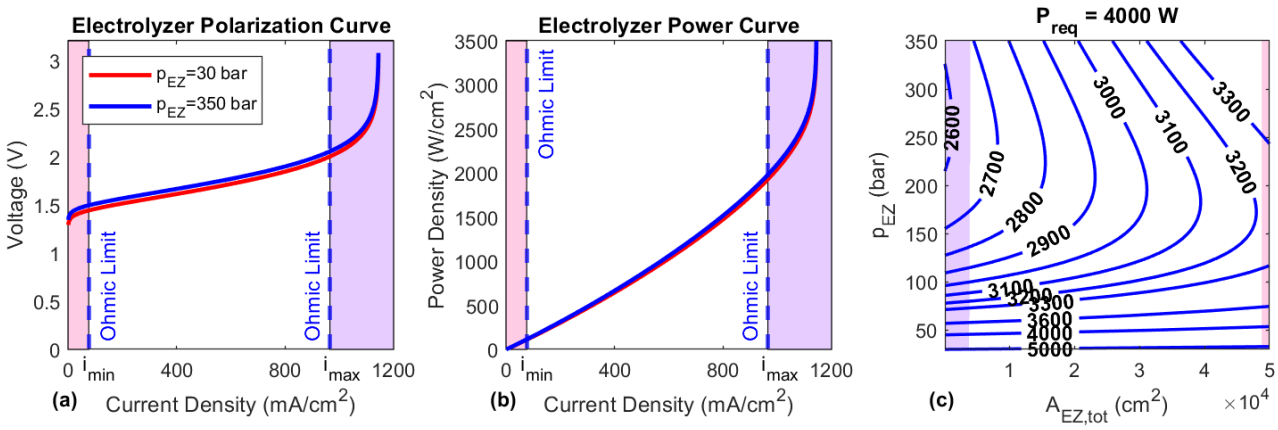

Figure 6: Electrolyzer Operation Graphs: (a) Electrolyzer polarization curve, (b) Electrolyzer power density curve, (c) Contour plot of total system mass m_{sys} for electrolyzer pressure and total area. The purple region corresponds to where the electrolyzer high voltage constraint is violated, and the pink region corresponds to where the low current density constraint is violated. This graph corresponds to $P_{req} = 4000$ W, $A_{FC,tot} = 22500$ cm^2, and $p_{FC} = 1.2$ bar.

The same three loss mechanisms appear as in the fuel cell: activation, ohmic, and concentration. The key distinction is their effects on the operating voltage. In a fuel cell, these losses reduce the operating voltage below V_{rev}, whereas in electrolysis they increase the required voltage above V_{rev}, requiring additional electrical energy to drive the reaction.

Because high cell voltage can promote undesirable side reactions and accelerate material degra-

dation, the electrolyzer voltage is constrained by a maximum allowable value,

$$V_{EZ} \leq V_{EZ,max}, \tag{2.53}$$

where $V_{EZ,max}$ is set to 2 V in this model.

The efficiency of the electrolyzer can be described using the ideal power consumed divided by the actual power consumed:

$$\eta_{EZ} = \frac{P_{ideal}}{P_{EZ}} = \frac{V_{rev}\, i_{EZ}\, A_{EZ,tot}}{V_{EZ}\, i_{EZ}\, A_{EZ,tot}} = \frac{V_{rev}}{V_{EZ}}. \tag{2.54}$$

Thus we find that the highest electrolyzer efficiency is achieved at low voltage and low current density.

As with the fuel cell, the electrolyzer current density must be limited to the ohmic region of the polarization curve. The admissible range is approximated by requiring that the second derivative of V_{EZ} with respect to i_{EZ} remains below a specified curvature tolerance, ϵ. Therefore, the current density is constrained to lie within the interval

$$i_{EZ} \in \left[\sqrt{\frac{\beta_{EZ}}{\epsilon}} - i_{EZ,offset},\ i_{EZ,lim} - \sqrt{\frac{c_{EZ}}{\epsilon}} \right]. \tag{2.55}$$

The optimal electrolyzer variables are governed primarily by the available solar power. Two regimes arise depending on the required power output P_{req}. At lower power levels, the electrolyzer power demand P_{EZ} remains below the available solar array power P_{SA}, and the input power constraint (Eq. (2.51)) is inactive. In this regime, electrolyzer power consumption does not influence the total system mass. Consequently, the total electrolyzer area $A_{EZ,tot}$ is chosen to minimize electrolyzer stack mass while satisfying the current density and voltage limits, and the operating pressure p_{EZ} is selected to reduce the combined mass of the electrolyzer, the reserved reactant gases, and the fluid tanks. In Figure 6, we can see that the minimizing value of the electrolyzer area $A_{EZ,tot}$ is where the high voltage constraint is binding, and the pressure is balanced at around 250 bar. The reserved reactant mass will be further discussed in Section 2.3.3, and the fluid tanks will be discussed in Section 2.3.4. At higher power levels, the solar array power constraint becomes active. In this regime, both the electrolyzer area and operating pressure must be adjusted to improve efficiency to meet gas production demands. Increasing the active area reduces the required current density, which lowers the cell voltage and decreases the electrolyzer power consumption, ensuring that the system remains within the available solar power limit.

2.3.3 Reserved Gases

To maintain gas flow without additional compressors, the maximum and minimum pressures of the reactant tanks are related to the operating pressures of the electrolyzer and fuel cell:

$$p_{tank,min} = 1.25 \cdot p_{FC}, \tag{2.56}$$

$$p_{tank,max} = 0.85 \cdot p_{EZ}. \tag{2.57}$$

The minimum tank pressure provides a safety margin above the fuel cell operating pressure to ensure a stable and reliable gas supply. The maximum tank pressure ensures that the electrolyzer outlet pressure remains higher than the tank pressure and allowing efficient refilling during operation.

The mass of reserved hydrogen gas can be determined using the universal gas law with the compressibility factor Z applied at the minimum tank pressure:

$$n_{H_2,res} = \frac{p_{tank,min} V_{H_2,in}}{R T_{temp} Z_{H_2}(T_{temp}, p_{tank,min})}, \tag{2.58}$$

where $n_{H_2,res}$ is the molar amount of the reserved hydrogen reactants, $V_{H_2,in}$ is the tank's internal volume, R is the universal gas constant, and T_{temp} is the tank temperature, assumed to be 25°C. The compressibility factor $Z_{H_2}(T_{temp}, p_{tank,min})$ accounts for deviations of hydrogen from ideal gas behavior as a function of temperature and pressure. A graph of Z_{H_2} versus pressure is shown in Fig. 7. The mass of the reserved hydrogen gas is obtained by multiplying the molar amount by the molar mass:

$$m_{H_2,res} = M_{H_2} n_{H_2,res} = M_{H_2} \frac{p_{tank,min} V_{H_2,in}}{R T_{temp} Z_{H_2}(T_{temp}, p_{tank,min})}. \tag{2.59}$$

Furthermore, when the tank is full, the expected pressure is $p_{tank,max}$, giving

$$m_{H_2,tot} = m_{H_2,res} + m_{H_2,cons} = M_{H_2} \frac{p_{tank,max} V_{H_2,in}}{R \cdot T_{temp} \cdot Z_{H_2}(T_{temp}, p_{tank,max})}. \tag{2.60}$$

Subtracting Eq. (2.59) from Eq. (2.60), yields

$$m_{H_2,cons} = M_{H_2} \frac{p_{tank,max} V_{H_2,in}}{R \cdot T_{temp} \cdot Z_{H_2}(T_{temp}, p_{tank,max})} - M_{H_2} \frac{p_{tank,min} V_{H_2,in}}{R \cdot T_{temp} \cdot Z_{H_2}(T_{temp}, p_{tank,min})}. \tag{2.61}$$

This allows us to relate $V_{H_2,in}$ with $m_{H_2,cons}$ as

$$V_{H_2,in} = \frac{m_{H_2,cons} R T_{temp}}{M_{H_2} \left(p_{tank,max}/Z_{H_2}(T_{temp}, p_{tank,max}) - p_{tank,min}/Z_{H_2}(T_{temp}, p_{tank,min}) \right)}. \tag{2.62}$$

Finally, we can substitute the tank volume from Eq. (2.62) back into Eq. (2.59) to calculate the reserved hydrogen mass.

For the oxygen reserve mass, the same approach is applied, replacing the hydrogen-specific constants with those for oxygen. This yields

$$m_{O_2,res} = M_{O_2} \frac{p_{tank,min} V_{O_2,in}}{R T_{temp} Z_{O_2}(T_{temp}, p_{tank,min})}, \tag{2.63}$$

$$V_{O_2,in} = \frac{m_{O_2,cons} R T_{temp}}{M_{O_2} \left(p_{tank,max}/Z_{O_2}(T_{temp}, p_{tank,max}) - p_{tank,min}/Z_{O_2}(T_{temp}, p_{tank,min}) \right)}, \tag{2.64}$$

completing the derivation of the reserved reactant masses.

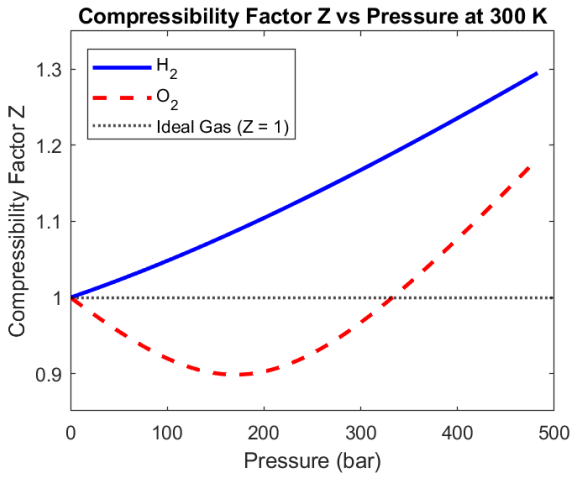

Figure 7: Compressibility Factor of H_2 and O_2 at 300 K

The mass of reserved reactant gases depends strongly on the operating pressures of the fuel cell and electrolyzer. According to Eq. (2.59), the reserve gas mass decreases with both lower fuel cell pressure and smaller tank volume. Although the compressibility factor also varies with pressure, its effect on the stored mass is relatively small compared to the direct influence of pressure. Equation (2.62) indicates that the tank volume is inversely proportional to the difference between the maximum and minimum tank pressures. Therefore, increasing the electrolyzer pressure or decreasing fuel cell pressure allows for a smaller tank volume, but increasing the electrolyzer pressure also increases the structural mass of the electrolyzer. The overall system design is determined by balancing reductions in stored reactant mass against the structural penalties associated with high-pressure operation as shown in Fig. 6.

2.4 Mass of Storage Tanks

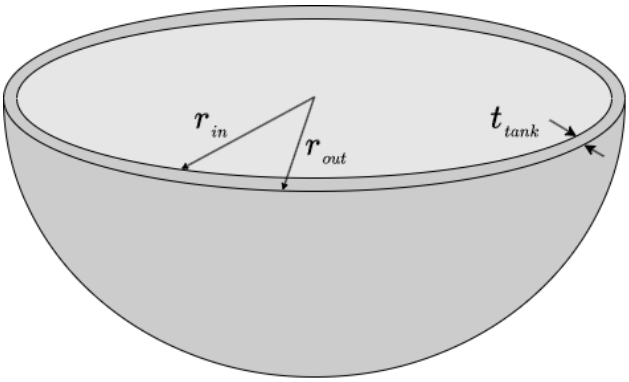

Figure 8: Spherical Tank Diagram

The balance-of-plant mass is the sum of the three storage tank masses (hydrogen, oxygen, and water):

$$m_{BoP} = m_{tank,H_2} + m_{tank,O_2} + m_{tank,H_2O}. \tag{2.65}$$

For simplicity, all tanks are assumed to be spherical containers, so the tank mass is

$$m_{tank} = \rho_{tank} \frac{4\pi}{3} \left(r_{out}^3 - r_{in}^3 \right), \tag{2.66}$$

where ρ_{tank} is the tank material density, while r_{in} and r_{out} are the inner and outer radii. The inner radius r_{in} is calculated by rearranging the equation for the volume of a sphere:

$$r_{in} = \left(\frac{3V_{in}}{4\pi} \right)^{1/3}, \tag{2.67}$$

where V_{in} is the required internal tank volume. The outer radius is calculated from the inner radius and the wall thickness.

$$r_{out} = r_{in} + t_{tank}. \tag{2.68}$$

Both the internal volume V_{in} and the tank thickness t_{tank} are calculated differently for the reactant gases and the water storage tanks.

For the hydrogen and oxygen gas tanks, we use the tank internal volume determined previously in Section 2.3.3, Eq. (2.62) and Eq. (2.64), ensuring the tanks will hold the maximum volume of the gas. A minimum thickness is required to prevent rupture under high pressure. For a thin-shell spherical container, one has [7]:

$$t_{tank,gas}^{min} = \frac{p_{tank,max}\, r_{in,gas}}{2\sigma_{stress}}, \tag{2.69}$$

where σ_{stress} is the allowable material stress, while $p_{tank,max}$ and $p_{tank,min}$ are the maximum and minimum tank pressures defined in Section 2.3.3. For conservatism and to conform with pressure-vessel practice, the minimum required wall thickness was calculated according to ASME BPVC Section VIII, Division 1, UG-27 [8]:

$$t_{tank,gas} = \frac{p_{tank,max}\, r_{in,gas}}{2\frac{YS}{SF} - 0.2\, p_{tank,max}}, \tag{2.70}$$

where YS is the material yield strength and SF is the safety factor (in this work $SF = 2$). The ASME form is used in the model as a conservative requirement; the thin-shell estimate above may be used for preliminary checks.

For the water tank, the maximum stored volume is determined by the combined mass of the reactants and converting to volume using the density of water:

$$V_{H_2O,in} = \frac{m_{H_2,cons} + m_{O_2,cons}}{\rho_{H_2O}}, \tag{2.71}$$

Since the water is incompressible, it is not necessary to store the water at high pressure, as it does not reduce the necessary volume. Thus, instead of calculating the water tank thickness from the internal pressure, a fixed radial thickness is chosen:

$$t_{tank,water} = 0.6 \text{ cm} \tag{2.72}$$

Since these tanks take up the most space in the system, the combined volume must be less than a maximum allowable volume:

$$V_{H_2,out} + V_{O_2,out} + V_{H_2O,out} \leq V_{tank,max}. \tag{2.73}$$

This constraint ensures the total system volume is sufficiently small to be transported.

2.5 Model Summary

To summarize the model, we minimize the total mass given by

$$m_{sys} = m_{FC} + m_{EZ} + m_{Gas} + m_{BoP}, \tag{2.74}$$

by varying eight independent variables within their ranges shown in Table 3.

For the fuel cell, we calculate the mass from the fuel cell variables:

$$m_{FC}(N_{FC}, k_{FC}, A_{FC}) = N_{FC}\left(a_1 A_{FC} k_{FC} + a_2\sqrt{A_{FC}}k_{FC} + a_3 A_{FC} + a_4\sqrt{A_{FC}} + a_5 k_{FC} + a_6\right), \tag{2.75}$$

Table 3: Model Variables

Variable	Description	Units	Range
A_{FC}	area of each cell in the fuel cell	cm^2	1 to 2000
k_{FC}	number of cells in the fuel cell	1	1 to 200
N_{FC}	number of fuel cells stacks	1	1 to 10
p_{FC}	pressure of the fuel cell	bar	1.2 to 7
A_{EZ}	area of each cell in the electrolyzer	cm^2	1 to 2000
k_{EZ}	number of cells in each electrolyzer	1	1 to 200
N_{EZ}	total number of electrolyzer stacks	1	1 to 10
p_{EZ}	pressure of the electrolyzer	bar	30 to 350

where a_1 through a_6 are all given.

For the electrolyzer mass, the equation is similar, but includes terms that are dependent on the electrolyzer pressure:

$$m_{EZ}(N_{EZ}, k_{EZ}, A_{EZ}, p_{EZ}) = N_{EZ}\Big(b_1\, k_{EZ}\, A_{EZ} + b_2\, k_{EZ}\, \left(r_{fr}^{EZ}\right)^2 + b_3\, A_{EZ}\, p_{EZ}\, k_{EZ} + b_4\, A_{EZ}\, p_{EZ} + b_5\, A_{EZ}\, p_{EZ}^{4/3}\left(r_{fr}^{EZ}\right)^{4/3} + b_6\, p_{EZ}^{1/3}\left(r_{fr}^{EZ}\right)^{10/3} + b_7\Big). \tag{2.76}$$

where

$$r_{fr}^{EZ}(A_{EZ}) = \alpha_{EZ}\sqrt{\frac{A_{EZ}}{\pi}} + r_{ext}^{EZ}. \tag{2.77}$$

Here b_1 through b_7 are given.

The gas mass is calculated as follows:

$$m_{Gas} = m_{H_2,cons} + m_{O_2,cons} + m_{H_2,res} + m_{O_2,res}. \tag{2.78}$$

We can reduce some of the fuel cell variables to a single variable for ease of calculation:

$$A_{FC,tot} = A_{FC}\, k_{FC}\, N_{FC}. \tag{2.79}$$

For the consumed reactant gas mass we calculate them using the mass transfer of the fuel cell:

$$m_{H_2,cons}(A_{FC,tot}, p_{FC}) = \frac{M_{H_2}}{n_{H_2} F}\, T_{FC}\, i_{FC}\, A_{FC,tot}, \tag{2.80}$$

$$m_{O_2,cons}(A_{FC,tot}, p_{FC}) = \frac{M_{O_2}}{n_{O_2} F}\, T_{FC}\, i_{FC}\, A_{FC,tot}, \tag{2.81}$$

where M_{H_2} and M_{O_2} are the molar masses of hydrogen and oxygen respectively, while n_{H_2} and n_{O_2} are moles of electrons transferred per mole of hydrogen and oxygen. The constant F is Faraday's constant while T_{FC} is the fuel cell operating time. The current density i_{FC} is solved from the required output power P_{req}:

$$i_{FC} V_{FC}(i_{FC}, p_{FC}) = \frac{P_{req}}{A_{FC,tot}}, \tag{2.82}$$

where the fuel cell voltage is determined from the polarization curve Eq. (2.41). We require that the current density lies within the following range, which ensures the voltage and current density are within the ohmic region of the polarization curve:

$$i_{FC} \in \left[\sqrt{\frac{\beta_{FC}}{\epsilon_{FC}}} - i_{FC,offset},\ i_{FC,lim} - \sqrt{\frac{c_{FC}}{\epsilon_{FC}}} \right]. \tag{2.83}$$

The reserve gas is calculated as follows:

$$m_{H_2,res}(A_{FC,tot}, p_{FC}, p_{EZ}) = M_{H_2} \frac{p_{tank,min} V_{H_2,in}}{R T_{temp} Z_{H_2}(T_{temp}, p_{tank,min})}, \tag{2.84}$$

$$m_{O_2,res}(A_{FC,tot}, p_{FC}, p_{EZ}) = M_{O_2} \frac{p_{tank,min} V_{O_2,in}}{R T_{temp} Z_{O_2}(T_{temp}, p_{tank,min})}, \tag{2.85}$$

where constant R is the universal gas constant and the temperature of the tank T_{temp} is assumed to be 25°C. The compressibility factors Z_{O_2} and Z_{H_2} are calculated from the tank pressure and temperature using the van der Waals equation of state. The inner tank volumes, $V_{O_2,in}$ and $V_{H_2,in}$, are calculated from the consumed gases:

$$V_{H_2,in} = \frac{m_{H_2,cons}(A_{FC,tot}, p_{FC})\, R\, T_{temp}}{M_{H_2} \left(p_{tank,max}/Z_{H_2}(T_{temp}, p_{tank,max}) - p_{tank,min}/Z_{H_2}(T_{temp}, p_{tank,min}) \right)}, \tag{2.86}$$

$$V_{O_2,in} = \frac{m_{O_2,cons}(A_{FC,tot}, p_{FC})\, R\, T_{temp}}{M_{O_2} \left(p_{tank,max}/Z_{O_2}(T_{temp}, p_{tank,max}) - p_{tank,min}/Z_{O_2}(T_{temp}, p_{tank,min}) \right)}, \tag{2.87}$$

where the pressures are:

$$p_{tank,min} = 1.25 \cdot p_{FC}, \tag{2.88}$$

$$p_{tank,max} = 0.85 \cdot p_{EZ}. \tag{2.89}$$

For the balance of plant, we calculate the mass from the storage tanks of the reactants and

water:

$$
\begin{aligned}
m_{_{BoP}} &= m_{_{tank,H_2}} + m_{_{tank,O_2}} + m_{_{tank,H_2O}}, && (2.90)\\
m_{_{tank}} &= \rho_{_{tank}} \frac{4\pi}{3} \left(r_{_{out}}^3 - r_{_{in}}^3 \right), && (2.91)\\
r_{_{in}} &= \left(\frac{3V_{_{in}}}{4\pi} \right)^{1/3}, && (2.92)\\
r_{_{out}} &= r_{_{in}} + t_{_{tank}}. && (2.93)
\end{aligned}
$$

where the density of the tanks $\rho_{_{tank}}$ is based on the chosen tank material. For the reactant gases, the volume is calculated from Eqs. (2.86) and (2.87). The reactant tank thicknesses depend on the stresses from pressure:

$$t_{_{tank,gas}} = \frac{p_{_{tank,max}}\, r_{_{in,gas}}}{2\frac{YS}{SF} - 0.2\, p_{_{tank,max}}}, \tag{2.94}$$

where YS is the yield strength of the tank, and SF is a chosen factor of safety. For the water tank, the internal volume, $V_{_{H_2O,in}}$, is calculated from the masses of the consumed reactant gases, while the thickness is set to 0.6 cm:

$$
\begin{aligned}
V_{_{H_2O,in}} &= \frac{m_{_{H_2,cons}} + m_{_{O_2,cons}}}{\rho_{_{H_2O}}}, && (2.95)\\
t_{_{tank,water}} &= 0.6 \text{ cm} && (2.96)
\end{aligned}
$$

where $\rho_{_{H_2O}}$ is the density of water. The total tank outer volumes must remain less than a maximum volume to ensure the system remains small enough to fit the transportation requirements:

$$\frac{4}{3}\,\pi\, r_{_{out,H_2}}^3 + \frac{4}{3}\,\pi\, r_{_{out,O_2}}^3 + \frac{4}{3}\,\pi\, r_{_{out,H_2O}}^3 \leq V_{_{tank,max}}, \tag{2.97}$$

Having defined the storage constraints, power limits are enforced on the electrolyzer. The electrolyzer power must remain below the available solar array power:

$$P_{_{EZ}} \leq P_{_{SA}}. \tag{2.98}$$

Similar to the fuel cell, we can reduce some of the electrolyzer variables to a single variable:

$$A_{_{EZ,tot}} = A_{_{EZ}}\, k_{_{EZ}}\, N_{_{EZ}}. \tag{2.99}$$

The electrolyzer power is calculated from the current density $i_{_{EZ}}$ and the voltage $V_{_{EZ}}$:

$$P_{_{EZ}}(A_{_{EZ,tot}}, i_{_{EZ}}, p_{_{EZ}}) = i_{_{EZ}}\, V_{_{EZ}}(i_{_{EZ}}, p_{_{EZ}})\, A_{_{EZ,tot}}, \tag{2.100}$$

where the voltage is calculated from the electrolyzer polarization curve Eq. (2.52), and the current density is determined from the fuel cell current density:

$$i_{EZ} = i_{FC} \frac{A_{FC,tot}\, T_{FC}}{A_{EZ,tot}\, T_{EZ}}. \tag{2.101}$$

The electrolyzer current density must also lie within the following bounds:

$$i_{EZ} \in \left[\sqrt{\frac{\beta_{EZ}}{\epsilon_{EZ}}} - i_{EZ,offset},\ i_{EZ,lim} - \sqrt{\frac{c_{EZ}}{\epsilon_{EZ}}} \right], \tag{2.102}$$

while the voltage must not exceed a maximum, to prevent overpotential:

$$V_{EZ} \leq V_{EZ,max}. \tag{2.103}$$

CHAPTER 3

Results

This chapter presents the optimization algorithm and corresponding results over a range of required power values P_{req}. For each P_{req}, the model determines the optimal system configuration that minimizes total mass while satisfying all governing constraints.

3.1 Algorithm

The optimization is performed using MATLAB's *fmincon* function, which requires the objective function and the constraint functions as its inputs, as well as the initial values of the design parameters we are looking to optimize. When using the eight individual parameters directly, we found that the program runs very inefficiently. In order to accelerate the process, we reduce the input parameters to four variables: $A_{FC,tot}$, p_{FC}, $A_{EZ,tot}$, and p_{EZ}. In Section 2.5, we observe that while the fuel cell mass depends on the individual independent variables A_{FC}, k_{FC}, and N_{FC}, the reactant mass and the tank masses depend only on the total fuel cell area. Thus we can map these variables to a single variable $A_{FC,tot} = A_{FC}\, k_{FC}\, N_{FC}$. Similarly, we can simplify the electrolyzer independent variables to a single variable $A_{EZ,tot} = A_{EZ}\, k_{EZ}\, N_{EZ}$.

Fig. 10 shows the optimal A_{FC}, k_{FC}, N_{FC}, and m_{FC} for the fuel cell in terms of $A_{FC,tot}$. Fig. 11 shows the optimal A_{EZ}, k_{EZ}, N_{EZ}, and m_{EZ} for the electrolyzer in terms of $A_{EZ,tot}$ and p_{EZ}. All of the optimal variables and masses are increasing functions of total area and pressure.

To implement the optimization, we have a two-step process. For the first step, we determine the individual parameters for the fuel cell unit (A_{FC}, k_{FC}, and N_{FC}) which minimize the fuel cell mass m_{FC} using *fmincon*, with $A_{FC,tot} = A_{FC}\, k_{FC}\, N_{FC}$ and the parameter ranges shown in Table 3 as the constraints. The electrolyzer unit's individual parameters can be determined similarly. Note that while the fuel cell mass m_{FC} is independent of the pressure p_{FC}, the electrolyzer mass m_{EZ} depends on both A_{EZ} and p_{EZ}. Also, these design parameters are independent of other parameters like P_{SA}, T_{FC}, etc., and only depend on the fuel cell and electrolyzer material parameters. Fig. 9 (a)

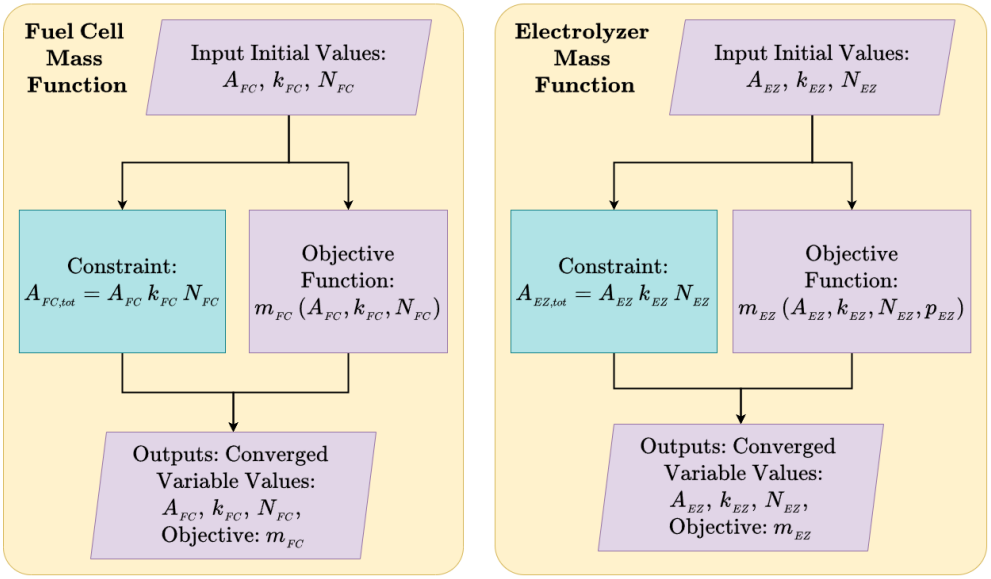

Figure 9: Fuel Cell and Electrolyzer Mapping Flowcharts.

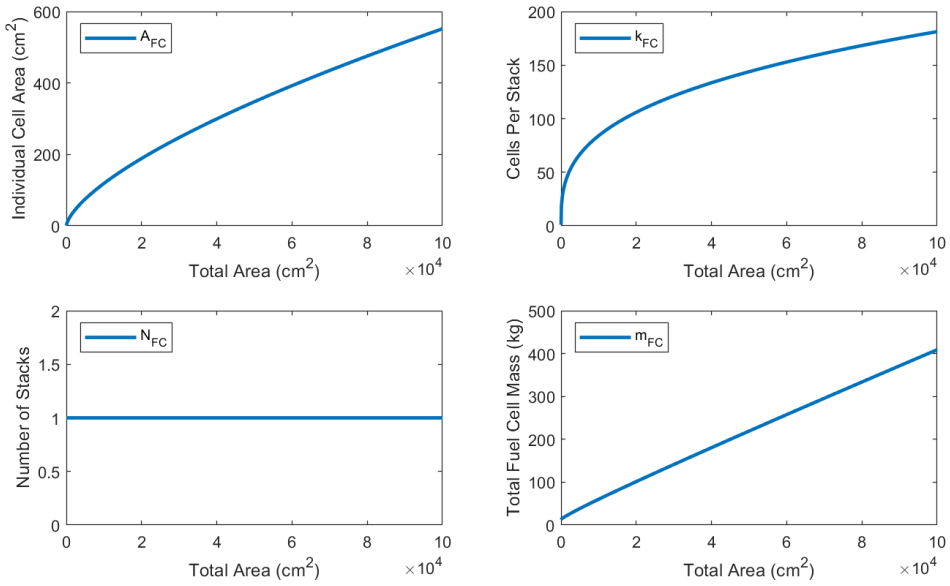

Figure 10: Optimal fuel cell variables for range of total fuel cell area $A_{FC,tot}$.

and 9(b) show the flow of these algorithms. The masses m_{FC} and m_{EZ} are precalculated and saved as a search table, so that the algorithm can quickly refer to this table for faster calculation of these masses.

In the second step, we calculate the mass of the reactant gas m_{gas} and the tank masses m_{BoP} with the given input parameters, and evaluate the constraint functions as shown in Fig. 12 (a). In

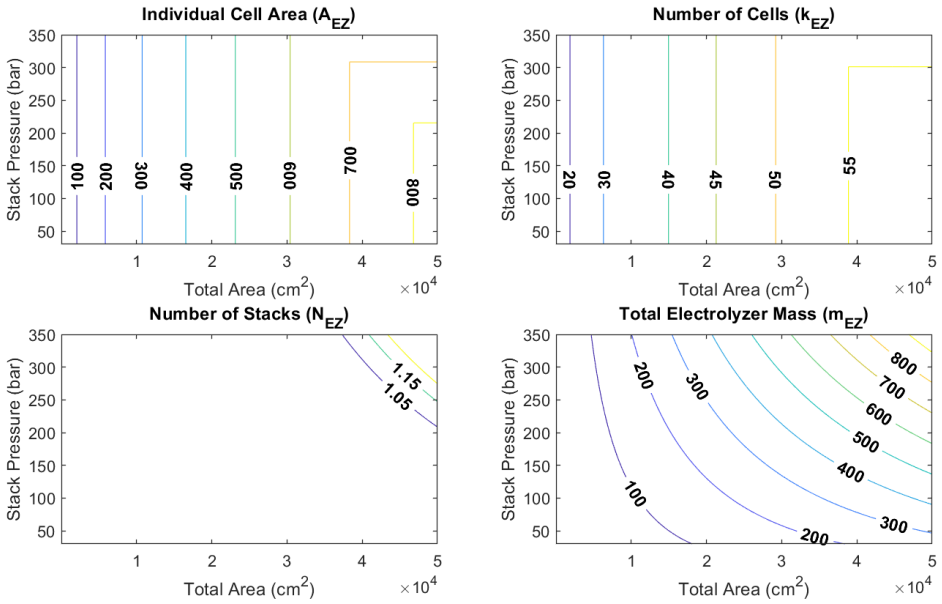

Figure 11: Contours of optimal electrolyzer variables for range of total electrolyzer area $A_{EZ,tot}$ and electrolyzer pressure p_{EZ}.

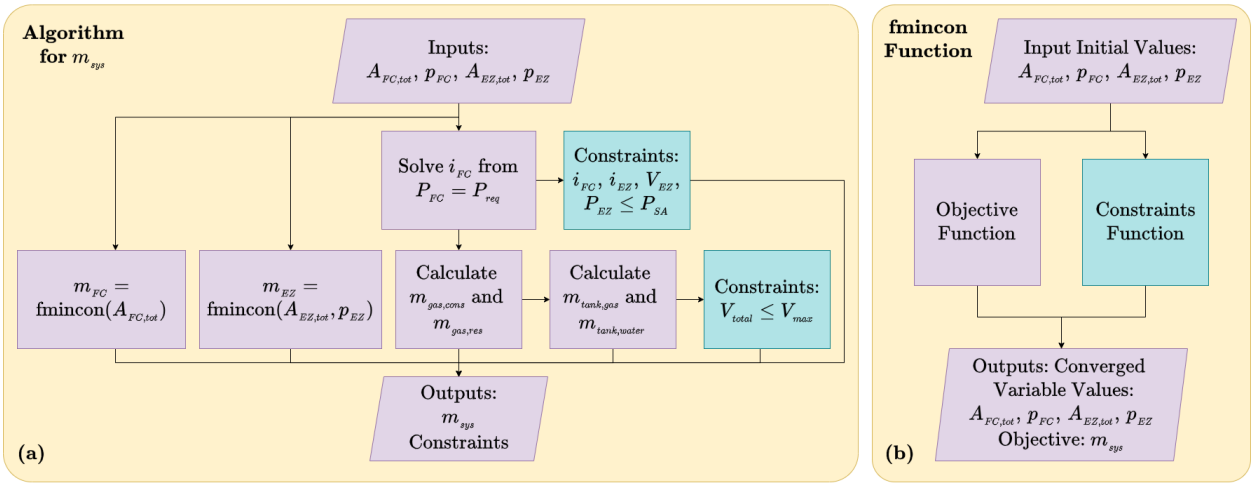

Figure 12: (a) Flowchart of Algorithm for calculating system mass, (b) Flowchart of *fmincon*.

this process, the current density i_{FC} must be solved using Newton's method from the requirement $P_{req} = P_{FC}$, while the calculations for the reactant gas and the storage tanks are straightforward evaluations. Now, for any given input, the algorithm gives us the constraint function values and four mass components, which are combined into a single value, total system mass m_{sys}.

The total mass and constraint functions are fed into *fmincon*, along with initial values of the four

variables. *fmincon* then gives the final converged result. To ensure we have a global minimizer, we input multiple initial values into *fmincon*. We use MATLAB's *lhsdesign* to produce a range of values for all four variables, using Latin hypercube sampling to give us relatively uniformly distributed values. We check each sample against the constraints, and use any feasible samples as the initial conditions input into *fmincon*.

3.2 Numerical Results

The results of the optimization for $P_{SA} = 10000$ W, $T_{EZ} = 351$ h, and $T_{FC} = 359$ h are shown in Figures 13–15 for $P_{req} \in [500, 7100]$ W [9, 2]. The numerical results show that the total system mass (Fig. 13(a)) increases monotonically with P_{req}. In contrast, the specific energy (Fig. 13(b)) exhibits a non-monotonic trend and reaches a maximum value of 535 W/kg at the critical power level $P^*_{\text{req}} = 5400$ W. This transition point corresponds to the onset of the active electrolyzer power constraint, indicating an optimal operating condition for the overall system performance.

For the fuel cell subsystem, increasing the required power P_{req} is achieved by increasing $A_{FC,tot}$ (Fig. 13(c)), while p_{FC} remains at its lower bound (Fig. 13(d)). Although increasing p_{FC} affects the achievable power through its impact on the operating voltage, it is not sufficient to satisfy the required power constraint over the full operating range on its own. In addition, increasing p_{FC} also increases both reactant consumption and tank mass. As a result, the optimal solution maintains p_{FC} at its lower bound while scaling power through $A_{FC,tot}$.

The optimal values for the electrolyzer subsystem exhibit a markedly different behavior in response to increasing P_{req}. The total electrolyzer area $A_{EZ,tot}$ is governed by Eqs. (2.49)–(2.51). For $P_{req} < P^*_{req}$, the power constraint is inactive and $A_{EZ,tot}$ increases approximately linearly. For $P_{req} > P^*_{req}$, the system is instead governed by the coupled balance between reactant production/consumption and the available power constraint,

$$i_{EZ}\, A_{EZ,tot} T_{EZ} = i_{FC}\, A_{FC,tot}\, T_{FC}, \qquad V_{EZ}\, i_{EZ}\, A_{EZ,tot} = P_{SA}, \tag{3.1}$$

which leads to

$$V_{EZ}(i_{EZ}, p_{EZ}) = \frac{P_{SA}\, T_{EZ}}{i_{FC}\, A_{FC,tot}\, T_{FC}}. \tag{3.2}$$

Accordingly, V_{EZ} decreases (Fig. 15(d)). Since the pressure dependence is weak, this reduction is achieved primarily by decreasing i_{EZ} (Fig. 15(c)), which necessitates a sharp increase in $A_{EZ,tot}$ to

maintain the required production rate (Fig. 13(c)).

The electrolyzer pressure p_{EZ} reflects a trade-off between stack and storage mass. Below P^*_{req}, increasing p_{EZ} reduces storage and tank mass with minimal impact on stack performance, leading to a slight increase in pressure. Above P^*_{req}, the system becomes power-constrained and stack mass dominates; since higher p_{EZ} increases stack mass, p_{EZ} decreases (Fig. 13(d)) while $A_{EZ,tot}$ increases to compensate for the reduced current density. This behavior is also illustrated in Fig. 14.

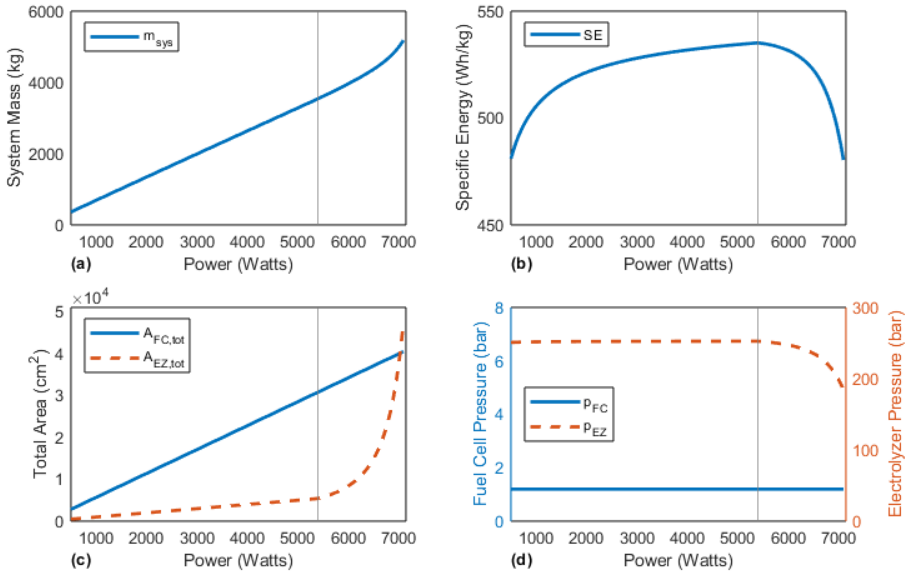

Figure 13: System Properties VS Power: (a) Total System Mass, (b) System Specific Energy, (c) Total Active Areas of Stacks: $A_{FC,tot}$ and $A_{EZ,tot}$, (d) Stack Pressures: p_{FC} and p_{EZ}.

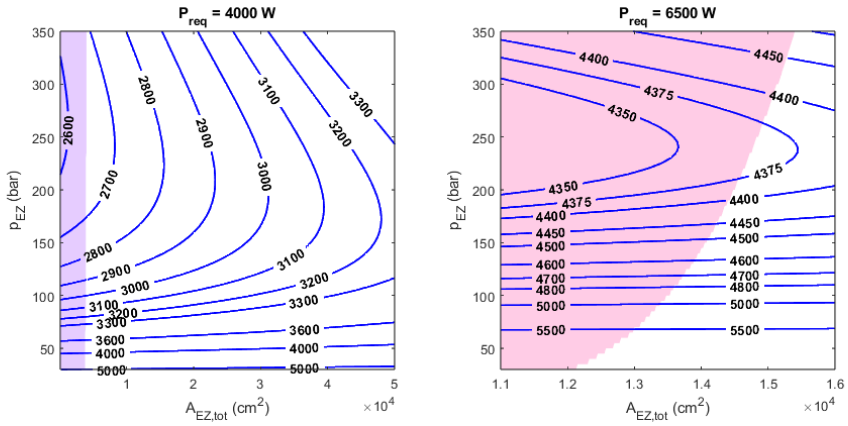

Figure 14: Total system mass contour plot.

The fuel cell variables exhibit consistent behavior, with voltage and current density fixed at the lower bound. The fuel cell power and mass increase linearly with P_{req}, while A_{FC} and k_{FC} scale proportionally with $A_{FC,tot}$. The electrolyzer variables follow similar trends below P^*_{req}; above it, m_{EZ}, A_{EZ}, and k_{EZ} increase more rapidly with P_{req}, consistent with the increase in $A_{EZ,tot}$.

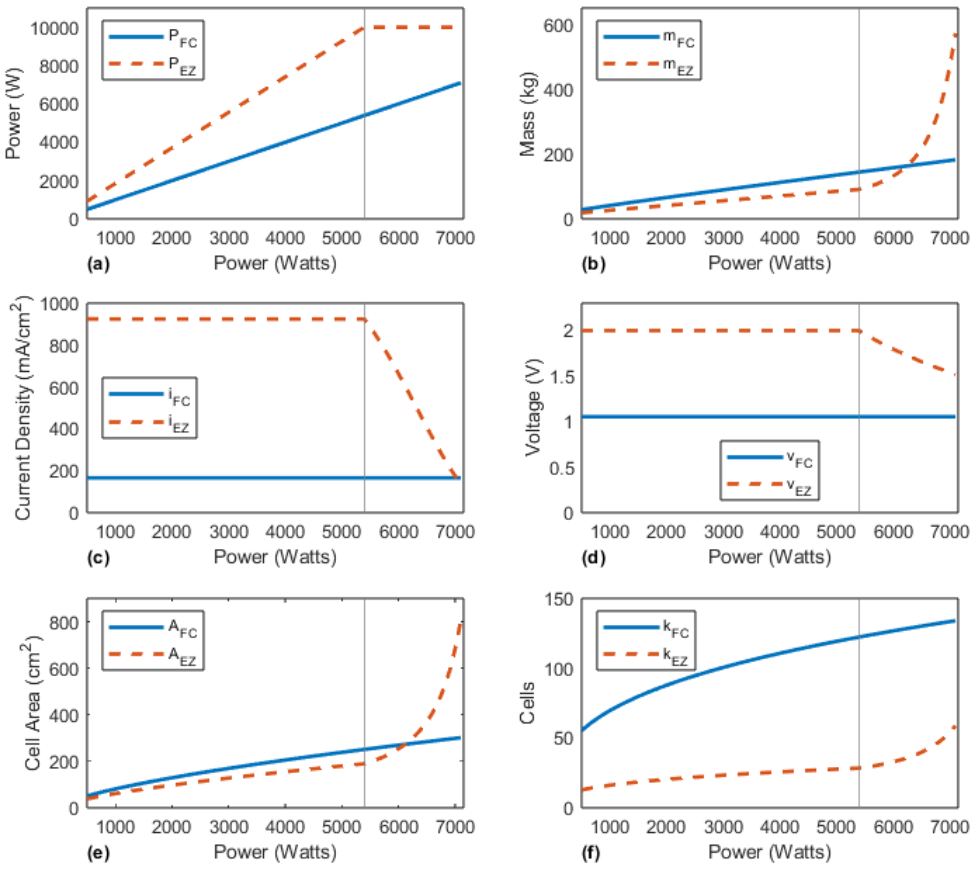

Figure 15: Stack Design Variables VS Power: (a) Stack Power: P_{FC} and P_{EZ}, (b) Fuel Cell and Electrolyzer System Masses: m_{FC} and m_{EZ}, (c) Fuel Cell and Electrolyzer Current Densities: i_{FC} and i_{EZ}, (d) Fuel Cell and Electrolyzer Voltages: V_{FC} and V_{EZ}, (e) Individual Cell Area of Fuel Cell and Electrolyzer: A_{FC} and A_{EZ}, (f) Number of Cells per Stack of Fuel Cell and Electrolyzer: k_{FC} and k_{EZ}.

The reactant and tank properties are shown in Fig. 16. The total reactant and tank masses increase with P_{req}, with tank mass remaining larger. Both consumed and reserve reactant masses

increase, with the reserve mass growing more rapidly at higher P_{req} due to the decrease in p_{EZ}. As tank sizing depends inversely on pressure, decreasing p_{EZ} leads to more rapid increases in tank radii and volumes. The tank thickness increases with P_{req}, then its growth slows beyond P^*_{req} and decreases after $P_{req} \approx 6150$ W, when the pressure term dominates Eq. (2.70). Note that although the hydrogen tank volume and mass are larger than that of oxygen, the oxygen reactant mass is greater.

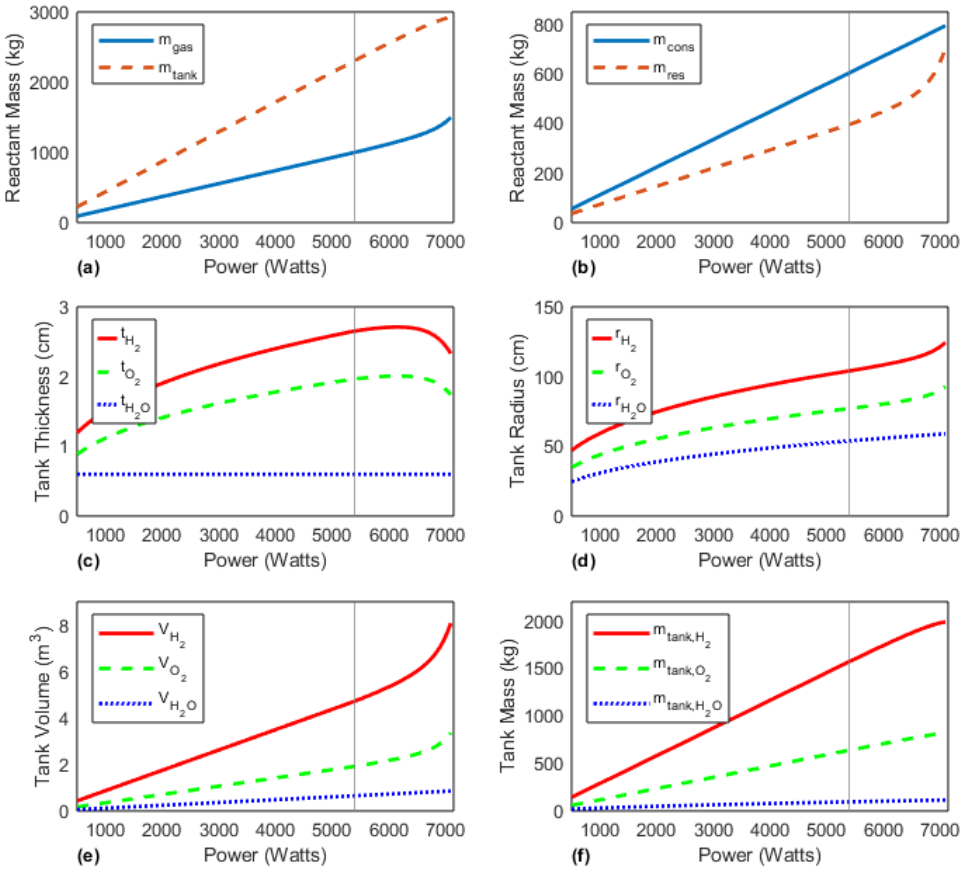

Figure 16: Tank and Reactant Gas Properties VS Power: (a) Total Reactant and Tank Mass (b) Consumed and Reserved Reactant Mass, (c) Tank Thickness, (d) Tank Radius, (e) Tank Volume, (f) Individual Tank Masses.

Table 4 lists the optimal system parameters at $P^*_{req} = 5400$ W. Note that the system was optimized without the integer constraint on the number of cells in the fuel cell and electrolyzer,

thus the optimum in reality will be slightly different since a partial cell is impractical.

Table 4: Parameter Values at $P_{req} = 5400$ W, $P_{SA} = 10000$ W, $T_{EZ} = 351$ h, and $T_{FC} = 359$ h.

System-Level Metrics					
SE	m_{sys}	$A_{FC,tot}$	$A_{EZ,tot}$	p_{FC}	p_{EZ}
535.2 W/kg	3542 kg	30780 cm^2	5423 cm^2	1.2 bar	252.7 bar
Fuel Cell Parameters					
A_{FC}	k_{FC}	N_{FC}	i_{FC}	v_{FC}	m_{FC}
251.5 cm^2	122.4	1	166.3 mA/cm^2	1.054 V	144.4 kg
Electrolyzer Parameters					
A_{EZ}	k_{EZ}	N_{EZ}	i_{EZ}	v_{EZ}	m_{EZ}
190.1 cm^2	28.53	1	923.0 mA/cm^2	2.00 V	91.14 kg
Hydrogen Mass and Tank Parameters					
$m_{H_2,cons}$	m_{tank,H_2}	$m_{H_2,res}$	t_{H_2}	r_{H_2}	V_{H_2}
67.72 kg	1.57 kg	53.04 kg	2.65 cm	104.1 cm	4.72 m^3
Oxygen Mass and Tank Parameters					
$m_{O_2,cons}$	m_{tank,O_2}	$m_{O_2,res}$	t_{O_2}	r_{O_2}	V_{O_2}
536.4 kg	639.1 kg	342.7 kg	1.97 cm	77.13 cm	1.92 m^3
Water Tank / Totals					
m_{tank,H_2O}	t_{H_2O}	r_{H_2O}	V_{H_2O}	$m_{tank,tot}$	$V_{tank,tot}$
96.78 kg	0.6 cm	53.95 cm	0.66 m^3	2306 kg	7.30 m^3

CHAPTER 4

Conclusion

This work develops a system-level model of a regenerative fuel cell (RFC) system to optimize specific energy for long duration, off-world energy storage applications. The model integrates four subsystems, namely the fuel cell, electrolyzer, reactant gases, and storage tanks, into a unified optimization framework in which subsystem sizing and operating pressures are coupled through required and available power, reactant production and consumption balance, and pressure-dependent storage tank sizing.

The mass of the fuel cell is modeled based on geometric design and material properties depending on the cell active area, number of cells per stack, and number of stacks. The electrolyzer model follows the same framework but also includes stack operating pressure as a design variable. Higher operating pressures increase structural requirements and therefore result in higher stack mass.

The mass of reactant gases is divided into two parts. The consumed gases in the fuel cell are based on the required mission power and operating time, while the produced gases in the electrolyzer must match the same quantity during the charging phase, and are constrained by the available power from the solar array and operation duration. The masses of consumed and produced gases are modeled using Faraday's law of electrolysis together with the electrical power relation, while the operating behavior of the fuel cell and electrolyzer is described using their respective polarization curves. On the other hand, the reserved gases in the tanks, which ensure no backflow in the system, are determined by the pressure difference between the fuel cell and electrolyzer, using the real gas law with a compressibility factor. Together, the consumed (equivalently the produced) and the reserved gases define the total required hydrogen and oxygen masses, and are used to compute storage volumes.

The masses of the storage tanks are calculated from storage volume and thickness. The thickness of the water tank is fixed, while the thickness of the gas tanks is calculated using a thin-shell

spherical model to prevent rupture under high pressure. This leads to a strong dependence of tank mass on the pressures of the fuel cell and electrolyzer.

The convergence of *fmincon* is negatively affected by sensitivity to strong nonlinear coupling between subsystems and the need for repeated evaluation of computationally expensive models. These issues are addressed through a reformulated problem structure and supporting code architecture. The primary strategy is to reduce the design space by consolidating lower-level design variables into total active area, with the corresponding subsystem behavior precomputed and stored in lookup tables. In this way, the variable compression and lookup table approach are unified: the lookup tables enable elimination of internal design variables while preserving the underlying physics. This significantly reduces both problem dimensionality and per-iteration computational cost. This enabled the model to converge on a viable answer out of a large discontinuous field.

To improve robustness, reduce sensitivity to local minima and constraint interactions, and increase the likelihood of global optimality, a multi-start strategy is employed. Initial conditions for *fmincon* are generated using Latin hypercube sampling to produce a well-distributed set of points across the design space. These samples are then filtered to retain only feasible points that satisfy all constraints. Each feasible sample is used as an initial guess for a separate *fmincon* run. This approach improves coverage of the feasible region and increases the likelihood of identifying a global or near-global optimum without modifying the underlying solver.

Together, the reduced design-space formulation with lookup-table-based subsystem evaluation and the multi-start initialization strategy enable *fmincon* to converge to the global minimum. This is critical for solving the optimization problem, given its high dimensionality and strongly nonlinear, coupled nature.

The numerical results show that maximum specific energy occurs at a critical required mission power, at which the electrolyzer power matches the solar array output and the electrolyzer operates near its upper limits of voltage and current density. At this point, the available power is fully utilized, minimizing the mass per unit of stored energy. Further increases in required power cause less mass-efficient electrolyzer operation, increasing system mass and reducing overall performance.

Several areas remain for future work. In particular, more detailed modeling of system losses should be included, such as reactant crossover and back-diffusion during operation, as well as storage losses including leakage or venting, since these effects would alter the required reactant

mass and tank sizing. Additional subsystems, particularly thermal management and electrical power systems, should also be incorporated. Thermal management is critical, as both the fuel cell and electrolyzer generate significant waste heat that must be rejected. Associated hardware (e.g., radiators, heat exchangers, coolant loops) can contribute substantially to system mass. Similarly, power management and distribution systems, including power electronics and control hardware, may introduce additional mass and efficiency losses depending on operating conditions. Finally, incorporating auxiliary fluidic components (e.g., pumps, valves, and flow control hardware) and accounting for parasitic power consumption would further improve fidelity, as these effects reduce net system efficiency and increase total system mass.

Further improvements could be achieved through reduced-order or simplified modeling to decrease computational cost while maintaining accuracy. Machine learning methods also offer a potential acceleration pathway; for example, a neural network trained on high-fidelity model outputs could approximate optimal design variables or system performance, reducing the need for repeated *fmincon* evaluations.

APPENDIX A

Nomenclature

Roman Symbols

Symbol	Description	Units
A	Active cell area	cm^2
A_{tot}	Total active area	cm^2
$a_1, \ldots, a_6$	Fuel cell mass model coefficients	varies
$b_1, \ldots, b_7$	Electrolyzer mass model coefficients	varies
c	Concentration loss coefficient	V
E	Elastic modulus	N/cm^2
F	Faraday constant	C/mol
i	Current density	mA/cm^2
i_0	Reference current density	mA/cm^2
i_{lim}	Limiting current density	mA/cm^2
i_{offset}	Current density offset	mA/cm^2
k	Number of cells per stack	–
k_{bolt}	Number of clamping bolts	–
m	Mass	kg
M	Molar mass	kg/mol
n	Number of moles	mol
$\dot{n}_e$	Electron molar flow rate	mol/s
n_{H_2}	Electrons transferred per mole of hydrogen	–
n_{O_2}	Electrons transferred per mole of oxygen	–
N	Number of stacks	–
P	Power	W

Symbol	Description	Units
P_{cons}	Internal power consumed during fuel cell operation	W
P_{ideal}	Ideal electrochemical power	W
P_{req}	Required gross power	W
P_{SA}	Available solar array power	W
p	Pressure	bar
p_0	Reference pressure	bar
R	Universal gas constant	J/(mol K)
R_{FC}	Fuel cell ohmic resistance term	Ω cm^2
R_{EZ}	Electrolyzer ohmic resistance term	Ω cm^2
r	Radius	cm
r_{in}	Inner tank radius	cm
r_{out}	Outer tank radius	cm
s	Maximum clamp force per bolt	N
SE	Specific energy per cycle	Wh/kg
SF	Factor of safety	–
T	Operating time	h
T_{temp}	Temperature	K
t	Thickness	cm
V	Cell voltage	V
V_{in}	Internal tank volume	cm^3
V_{out}	Outer tank volume	cm^3
V_{rev}	Reversible voltage	V
$V_{tank,max}$	Maximum allowable tank volume	cm^3
x	Optimization design variable vector	–
YS	Yield strength	N/cm^2
Z	Compressibility factor	–

Greek Symbols

Symbol	Description	Units
α	Geometric scaling factor	–
β	Activation loss coefficient	V
ΔG_F	Gibbs free energy of formation of water	J/mol
δ_{max}	Maximum allowable endplate deflection	cm
ϵ	Curvature tolerance parameter	V/cm^4
η	Electrochemical efficiency	–
ν	Poisson's ratio	–
ρ	Density	kg/cm^3
$\sigma_{_{MEA}}$	Area density	kg/cm^2
$\sigma_{_{stress}}$	Stress	N/cm^2
ϕ	Porosity	–

Subscripts and Superscripts

Symbol	Description
FC	Fuel cell
EZ	Electrolyzer
BoP	Balance of plant
Gas	Stored reactant gas subsystem
SA	Solar array
MEA	Membrane electrode assembly
bp	Bipolar plate
fr	Frame
ep	Endplate
aux	Auxiliary component
sc	Screen
an	Anode
ca	Cathode
$bolt$	Bolt

Symbol	Description
$tank$	Storage tank
H_2	Hydrogen
O_2	Oxygen
H_2O	Water
$cons$	Consumed
$prod$	Produced
res	Reserve
tot	Total
$ideal$	Ideal
rev	Reversible
lim	Limiting value
$offset$	Offset value
min	Minimum
max	Maximum
in	Inner or internal quantity
out	Outer quantity
0	Reference value
$*$	Optimal value

Abbreviations

Abbreviation	Description
RFC	Regenerative fuel cell
FC	Fuel cell
EZ	Electrolyzer
PEM	Proton exchange membrane
MEA	Membrane electrode assembly
BoP	Balance of plant
SE	Specific energy

Abbreviation	Description
LHS	Latin hypercube sampling
ASME	American Society of Mechanical Engineers
BPVC	Boiler and Pressure Vessel Code
PMAD	Power management and distribution

BIBLIOGRAPHY

[1] Phillip J. Smith, Kerrigan P. Cain, Ryan P. Gilligan, and Ian J. Jakupca. Lunar equator regenerative fuel cell system efficiency analysis. Technical Report NASA/TM-20210014627, NASA Glenn Research Center, 2022.

[2] Phillip J. Smith, Zhimin Zhong, Kerrigan P. Cain, Jessica L. Cashman, Bryan W. Debelak, Ryan P. Gilligan, David S. Hervol, Cody A. O'Meara, Robert D. Green, Erik J. Stalcup, and Ian J. Jakupca. Aerospace regenerative fuel cell fluidic component design challenges. Technical Report NASA/TM-20210024659, NASA Glenn Research Center, 2022.

[3] Ansel C. Ugural. *Stresses in Plates and Shells*. McGraw-Hill, New York, 1981.

[4] Richard G. Budynas and J. Keith Nisbett. *Shigley's Mechanical Engineering Design*. McGraw-Hill, 9th edition, 2014.

[5] Colleen Spiegel. *PEM Fuel Cell Modeling and Simulation Using MATLAB*. Academic Press, 2008.

[6] A review of hydrogen-based regenerative fuel cell systems for energy storage. *Renewable and Sustainable Energy Reviews*, 2023.

[7] James M. Gere and Barry J. Goodno. *Mechanics of Materials*. Cengage Learning, 9th edition, 2018.

[8] American Society of Mechanical Engineers. *ASME Boiler and Pressure Vessel Code, Section VIII, Division 1: Rules for Construction of Pressure Vessels*. American Society of Mechanical Engineers, New York, NY, 2023. See UG-27: Thickness of Shells Under Internal Pressure.

[9] National Aeronautics and Space Administration (NASA). Relocatable 10 kw solar array for lunar south pole missions. `https://techport.nasa.gov/projects/116305`, 2021. NASA TechPort Project ID: 116305.